Chronic pancreatitis patient-derived organoids reveal new paths to precision therapeutics

Victoria Osorio-Vasquez[1], Jonathan Zhu[1], Jan C. Lumibao[1], Kathryn Lande[1,2], Kristina L. Peck[1], McKenna K. Stamp[1], Shira R. Okhovat[1], Hyemin Song[1,3], Satoshi Ogawa[1], Casie Kubota[1], Vasiliki Pantazopoulou[1], Yang Dai[1], Angelica Rock[1], Chelsea Bottomley[1], Ethan Thomas[1], Jasper Hsu[1,3], Araceli Herrera Morales[1], Alexandra Fowler[1], T'Onj McGriff[1], K. Garrett Evensen[1], Siri Larsen[4], Muhamad Abdulla[4], Phil Greer[5], Jessica Gibson[5], Michael Downes[1], Ronald Evans[1], Andrew M. Lowy[6], David C. Whitcomb[5,7], Jingjing Zou[8], Alfredo Molinolo[9], Tae Gyu Oh[10], Rebekah White[6], Melena Bellin[4,11], Herve Tiriac[6], Dannielle D. Engle[1,3,*]

[1]Salk Institute for Biological Studies, La Jolla, CA, USA.
[2]Sanford Burnham Prebys Medical Discovery Institute, La Jolla, CA, USA
[3]School of Biological Sciences Department of Molecular Biology, University of California San Diego, School of Medicine, La Jolla, CA, USA
[4]Schulze Diabetes Institute, Department of Surgery, University of Minnesota Medical School, Minneapolis, MN, USA.
[5]Ariel Precision Medicine, Pittsburgh, PA, USA.
[6]Department of Surgery, Division of Surgical Oncology, Moores Cancer Center, University of California San Diego, San Diego, CA, USA.
[7]University of Pittsburgh, Pittsburgh, PA, USA.
[8]Herbert Wertheim School of Public Health and Human Longevity Science, University of California San Diego, CA, USA.
[9]Department of Pathology, Biorepository and Tissue Technology Shared Resource, Moores Cancer Center, UC San Diego, San Diego, CA, USA.
[10]University of Oklahoma, College of Medicine, Oklahoma City, OK, USA.
[11]Departments of Pediatrics, Division of Pediatric Endocrinology, University of Minnesota Medical School Minneapolis, MN, USA.

[*]Correspondence: engle@salk.edu

Summary

Chronic pancreatitis (CP) affects ~3 million people worldwide, yet altering the course of disease is challenging. We developed a patient-derived organoid (PDO) platform to investigate the molecular pathogenesis of this disease and identify therapeutic strategies. We generated 36 PDOs from patients with idiopathic, hereditary, and alcohol-related CP with high genetic concordance. PDOs retained inflammation-associated transcriptional and proteomic features. Transcriptomic profiling revealed three molecular subtypes of CP independent of etiology. We discovered widespread dysfunction of the cystic fibrosis transmembrane conductance regulator (CFTR) in half of the CP PDOs, including those with wildtype CFTR. Clinically available CFTR modulators stabilized mutant or wildtype CFTR, restored CFTR function, and decreased mitogenic and inflammatory signaling. This work provides the first comprehensive PDO platform for modeling CP. We demonstrate the utility of this platform for precision therapeutic investigations. Our findings reveal CFTR modulators as a broadly applicable and effective therapeutic strategy.

Keywords: chronic pancreatitis, patient derived organoids, CFTR, molecular subtypes, CFTR correctors, CFTR potentiators

Introduction

Pancreatitis, or pancreatic inflammation, is a continuum of diseases that may progress from acute to chronic stages. More than 300,000 Americans and 3 million individuals globally have chronic pancreatitis (CP)[1-3]. CP is characterized by atrophy, fibrosis, pancreatic exocrine insufficiency, diabetes mellitus, and intractable pain. Current treatment is largely supportive and often fails to modify disease progression, sometimes requiring surgical interventions such as partial or total pancreatectomy for pain management. CP may arise from numerous environmental and genetic factors. It is classified using the Toxic-metabolic, Idiopathic, Genetic, Autoimmune, Recurrent and severe acute pancreatitis and Obstructive (TIGAR-O v2) framework[4]. The most common identifiable causes of CP include tobacco use (46-60%)[5,6], gallstones (14-37%)[7,8], alcohol (7-34%)[5,9], and genetics (10%)[5], though a striking 28-80% of cases remain idiopathic[10]. Hereditary CP is associated with pathogenic germline mutations in protease serine 1 (*PRSS1*) (68-80%)[11-14], serine protease inhibitor kazal type 1 (*SPINK1*) (1-8.8%)[10-13], cystic fibrosis transmembrane conductance regulator (*CFTR*) (16.5%)[13], and other genes.

Pancreatitis initiation can be traced to dysfunction in both acinar and ductal cells. *PRSS1* and *SPINK1* mutations lead to hyperactivation of digestive enzymes, leading to acinar cell injury and inflammation[15-20]. Mutations in *CFTR* disrupt bicarbonate secretion in the pancreas. Ductal cells normally secrete 1-2L of 140mM sodium bicarbonate per day[21], which is essential for mucin production, flushing digestive enzymes into the duodenum, preventing premature digestive enzyme activation, and neutralizing acidic chyme from the stomach[21-23]. Unlike cystic fibrosis, CFTR variants associated with hereditary CP are often heterozygous[24]. Up to 37% of hereditary CP patients harbor *CFTR* mutations[25-32]. Importantly, 50% of idiopathic CP patients harbor *CFTR* alterations when extensive genotyping is performed[21,25-34]. Many *CFTR* variants associated with hereditary CP selectively impair bicarbonate, but not chloride transductance. Altogether, CFTR dysfunction in the pancreas, distinct from classical cystic fibrosis, may underlie a significant proportion of CP and represents an underexplored therapeutic target.

With more than 2,000 mutations annotated for *CFTR*, the response of most *CFTR* variants to modulators are unknown. Of those with response information, this testing has been primarily performed for cystic fibrosis-related variants in non-pancreas relevant contexts. Further, cystic fibrosis patient responses to CFTR therapies are highly variable due to undefined mechanisms[35-40]. Limited information is available regarding CFTR modulator response in the context of hereditary pancreatitis associated *CFTR* mutations. Delineating the genotypic and phenotypic relationships of pancreatitis-associated CFTR alterations with modulator response is essential. But these investigations have been hampered by the limited availability of renewable human models. Unfortunately, despite sharing 78% homology, mouse CFTR does not respond to human CFTR modulators, complicating mechanistic investigations in mouse models[41]. Further, mouse bicarbonate secretion is notably different than humans, reaching only 50mM in pancreatic secretions[37], limiting our ability to make conclusions relevant to human physiology.

Three-dimensional patient-derived organoids (PDOs) have emerged as transformative models for studying pancreas biology. PDOs can be generated from normal human pancreas and pancreatic ductal adenocarcinoma with high efficiency [42,43], far surpassing earlier monolayer or iPSC-based platforms[44]. PDOs are expandable, cryopreservable, and genetically stable, enabling in-depth molecular and functional analyses[43,45-50]. In pancreatic ductal adenocarcinoma (PDA), PDOs faithfully recapitulate transcriptomic and genetic subtypes, predict treatment response, and inform mechanisms of resistance[43,45-50]. Despite lacking a microenvironment, PDOs retain remarkable predictive power due to the central role of epithelial-intrinsic signaling in disease behavior[51,52]. PDO models of CP remain rare. A pediatric cohort (n=9) has been described[53], but generation efficiency, molecular fidelity, and translational potential remain unknown. To address this gap, we created a comprehensive biobank of CP PDOs encompassing all major etiologies and benchmarked their ability to model disease features and guide treatment strategies.

We report a high PDO generation success rate (70.5%, *n*=36) and strong concordance with

matched primary tissues at the DNA, RNA, and protein levels. Genetic analyses of 24 PDOs identified germline pathogenic variants in 2 out of 8 idiopathic cases. In addition, rare somatic variant analyses identified 2 CP PDOs with alterations associated with pancreatic ductal adenocarcinoma, including *KRAS* and *TP53*. These oncogenic alterations were not detectable in primary samples in which low cellularity limits the ability to detect somatic mutations in the epithelial compartment. CP PDOs exhibit elevated fibroinflammatory gene and protein expression profiles despite being removed from the pancreatic microenvironment, suggesting that ductal epithelial cell intrinsic features contribute to inflammation. Strikingly, half of the PDOs tested displayed CFTR functional impairment despite 2 out of the 4 dysfunctional lines harboring wildtype CFTR. Treatment with clinically available CFTR modulators restored ductal function and suppressed pro-inflammatory and mitogenic signaling, suggesting that CFTR modulation may benefit a broad segment of CP patients. Together, this study presents a robust and scalable platform for dissecting CP pathophysiology and accelerating precision medicine efforts.

Methods

Human Specimens

Normal pancreata were obtained from the Lifesharing organ donation program. The average age of the hNP PDOs is 56 years of age. Pancreatitis tissues were obtained from the University of Minnesota (UMN) and University of California San Diego (UCSD) Biorepository and Tissue Technology Shared Resource (BTTSR). De-identified pancreatitis tissues were obtained from the University of Minnesota (UMN) or the UCSD BTTSR with approval from their respective Institutional Review Boards. Written and informed consent or parental assent, as age appropriate, was obtained prior to acquisition of tissue from all patients. Age and/or age ranges will not be provided for pediatric patients as the rarity of the procedure in this patient population could itself be identifying. Specimens were obtained from patients with chronic pancreatitis at UCSD undergoing either partial pancreatectomy (distal pancreatectomy or pancreaticoduodenectomy) or pancreatic head debridement during pancreatic drainage procedures for symptomatic relief. Excess tissue was collected fresh into cold media for organoid generation. When available, pancreatic juice was collected in parallel by needle aspiration of pancreatic duct during drainage procedures. Specimens were obtained from patients undergoing total pancreatectomy and islet auto-transplantation at UMN. During pancreatectomy, the blood supply was preserved to the pancreas as long as possible to avoid prolonged ischemia. The entire pancreas, spleen, and duodenum were removed, and the gastrointestinal and biliary continuity is restored by a Roux-en-Y approach. Islet isolation was performed by infusing the pancreas with collagenase and neutral protease for enzymatic digestion, followed by mechanical disruption using the semi-automated method of Ricordi. The islets were then transported back to the operating room where they were infused via the portal vein on the same day as the pancreatectomy procedure. Residual exocrine pancreas tissue following islet isolation was collected for tissue research. Tissue specimens were catalogued, imaged, and processed (i.e. histology, organoid generation, flash frozen, and viably cryopreserved).

Histology and immunohistochemistry

Tissues were fixed in 10% neutral buffered formalin for 48 hours. Tissues were embedded in paraffin and stained with hematoxylin and eosin or Masson's trichrome by the Tissue Technology Shared Resource at UCSD supported by the National Cancer Institute Cancer Center Support Grant (CCSG Grant P30CA23100). The following primary antibodies were used for immunohistochemical staining Ki-67 (8D5, Cell Signaling Technologies# 9449), CK19 (Troma-III, Developmental studies hybridoma bank), CFTR (M3A7, Thermo Fischer #MA5-11768), Cancer Antigen 19-9 (MyBioSource #MBS850562). Secondary antibodies used were ImmPRESS® HRP Horse Anti-Mouse IgG Polymer Detection Kit (MP-7402) or ImmPRESS® HRP Goat Anti-Rat IgG Polymer Detection Kit (MP-7404) with ImmPACT® DAB Substrate Kit (HRP) (SK-4105). Staining intensity was semi quantitatively scored as: low, medium, or high using QuPath 0.5.0[54] and ranking percent positive staining. Slides were imaged using the Olympus VS-120 virtual slide scanning microscope, Olympus BX43 Microscope, or Zeiss Axioscan 7. Zen lite or CellSens was used to visualize and annotate images.

Pathologist Review of Patient Primary Tissue Specimen

Primary tissue specimen stained with hematoxylin and eosin or Masson's trichrome were scanned (Aperio-Leica AT2 Scanner, 40x) analyzed and imaged. Severity of fibrosis, acinar atrophy, inflammation and ductal changes were categorized as mild, moderate, or severe as denoted by dilation of ducts, expansion of fibroblast compartment, collagen deposition, and infiltration of

168 immune cells[55]. Alterations in histology due to autolytic changes or signs of cautery from an
169 electro-scalpel.
170
171 *Organoid generation and culture*
172
173 Prior to processing, visible fat, mesentery, and calcifications were removed. Patient specimens
174 were minced and aliquoted for viable tissue cryopreservation for potential regeneration of PDOs,
175 flash frozen for primary tissue DNA extraction, and further dissociation for PDO generation. For
176 organoid generation, tissue was minced and incubated in digestion media (3000 U/mL
177 Collagenase XI + 1000 U/mL hyaluronidase- Stem Cell #07919 in DMEM/F12 diluted 1:4 in
178 Advanced DMEM (Thermo Fischer #12634010) with 1% (v/v) glutamax (Thermo Fischer
179 #35050061), 1% (v/v) penicillin/streptomycin (Life Technologies #15140122), and 1%(v/v)
180 HEPES (1M, pH 7.5)) at 35°C while rotating. If cell lysis became apparent, DNAse I (10 µg/mL,
181 Roche #1128493200) was added. Fractions were collected every 20 minutes for up to 1 hour by
182 allowing large tissue pieces to sediment before supernatant was collected. Dissociation of the
183 remaining large tissue fragments continued by replacing the digestion media. Supernatant was
184 centrifuged at 300x RCF at 4°C for 5 minutes. The first fraction cell pellet collected was
185 resuspended in 1 mL of HBSS (Life Technologies #14175095) with 2% FBS and placed on ice
186 while collecting additional fractions from the digested tissue. After 3 fractions were collected, the
187 supernatant fractions were washed with Advanced DMEM with 1% (v/v) glutamax, 1% (v/v)
188 penicillin/ streptomycin, and 1% (v/v) HEPES prior to resuspension in Matrigel for plating. If larger
189 tissue pieces remained at the end of dissociation, they were either viably cryopreserved
190 (CrySOfree- Sigma-Aldrich #C9249) or plated in Matrigel (Corning #356231) in separate wells.
191 Cells were plated in Corning Matrigel from lots 28323001, 2011001, 0287001, and 1062004
192 during growth, expansion and experiments. Following Matrigel solidification, complete feeding
193 media was applied to each well.
194
195 Murine normal pancreas organoids were cultured in medium previously described[43,50]. Human
196 normal pancreas and human pancreatitis were cultured in human complete feeding medium.
197 Human complete feeding medium was prepared using Advanced DMEM/F12 containing HEPES
198 (1 % (v/v), 1M, pH 7.5), glutamax 1 % (v/v), B27 supplement (1x ,Life Technologies #A3582801),
199 and 1% (v/v) penicillin/streptomycin; N-acetylcysteine (1.25 mM, Sigma-Aldrich #A9165),
200 nicotinamide (10 mM, Thermo Fischer #125271000); hEGF (50 ng/mL, R&D Systems #236-EG),
201 FGF-10 (100 ng/mL, R&D Systems #345-FG), gastrin (10 nM, R&D #3006), and A83-01 (500 nM,
202 Tocris Bioscience #2939); rNoggin (100 ug/mL, Qkine LTD #Qk034) and rRSPO1 (10nM Qkine
203 LTD # Qk006); Wnt surrogate (300 pM, ImmunoPrecise Antibodies #N001); PGE2 (1 µM, Tocris
204 Bioscience #2296) and Y-27632 dihydrocholoride (10.5 µM, Tocris Bioscience #1254). Mouse
205 organoid media lacked Wnt3a, PGE2, and Y-27632 and utilized 10% RSPO1 conditioned media
206 and 10% Noggin conditioned media. Organoid nomenclature is defined as: hNP, human normal
207 pancreas; hCP, human chronic pancreatitis, mNP, mouse normal pancreas. All organoid models
208 were routinely tested for *mycoplasma* at Salk Institute.
209
210 *Whole mount immunofluorescence and EdU incorporation*
211
212 Organoids were cultured as described above in µ-slide (Ibidi #80826). Reagents for Click-iT Plus
213 EdU Cell Proliferation Kit for Imaging (Thermo Fischer #C10639) were used in accordance with
214 manufacturer's protocol. Organoids were treated with EdU for 25 hours by removing half of the
215 media and adding EdU containing media (20 µM). Matrigel domes containing organoids were
216 washed using PBS prior to fixing with 4% PFA (v/v) at 37°C for 10 minutes. After fixation rinsed
217 with excess 3% BSA and removed wash solution. Permeabilized with 0.5% Triton X-100 in PBS
218 for 10 minutes at room temperature. Steps subsequent to Click-it reaction cocktail addition were

219 protected from light. Remaining organoids were washed with 3% BSA in PBS and blocked with
220 IF buffer (0.1% Bovine serum albumin, 0.2% goat serum, 0.2% triton x-100, 0.05% Tween
221 20:sterile filtered + 10% Goat serum in PBS) for 1 hour. Organoids were incubated with a dilution
222 of 1:200 for CK-19 (Invitrogen #MA5-12663) overnight at room temperature. Organoids were
223 washed for 1 hour prior to incubation with secondary antibody (Jackson ImmunoResearch
224 Laboratories Inc. #115-545-003) and Hoechst for 2 hours at room temperature. Washed
225 organoids for at least 1 hour with IF buffer prior to mounting using Prolong Glass Antifade
226 Mountant (Thermo Fisher P36980) and dried overnight. Imaged using the Yokogawa CQ3000 at
227 20x. Nuclei and EdU positive nuclei were quantified using Cell Profiler (3.8.1)[56].
228
229 *Immunoblot*
230
231 Standard techniques were employed for immunoblotting (IB) of human organoids. Organoids
232 were isolated from Matrigel using cell recovery solution (10 mM HEPES 7.5 pH, 1x glutamax (v/v),
233 12.5 mM EDTA, 12.5 mM EGTA, 4.5 g/L dextrose in PBS w/o Ca and Mg) on ice with 0.5x
234 protease and phosphatase inhibitors (Thermo Fischer # PIA32961). After incubation on ice for 20
235 minutes, organoids were centrifuged at 0.8 x 1000 RCF at 4°C to pellet organoids and remove
236 cell recovery solution. Cell pellet was resuspended in TNET (1% (v/v) Triton X100, 150 mM NaCl,
237 5 mM EDTA, 50 mM Tris pH 7.5) with 1.0X protease and phosphatase inhibitors (Life
238 Technologies #A32961) and incubated on ice for 10 minutes before clarifying lysates for whole
239 cell lysate isolation. Protein quantification was carried out using BCA assay (Thermo Scientific
240 #23227). Protein lysates used to probe for CFTR were warmed to 37°C for 1 hour to prevent
241 insolubility, all other blots were performed using lysates heated to 95°C for 5 minutes. Protein
242 lysates were separated on a 4%-12% Bis-Tris NuPage gel (Invitrogen). Western blots were
243 probed with at a dilution of 1:1000 for CFTR (D6W6L, Cell Signaling Technologies #78335),
244 CA19-9 (MyBioSource #MBS850562), pEGFR (Y1068, Cell Signaling Technologies #3777),
245 EGFR (D38B1, Cell Signaling Technologies #4267), pSTAT3 (Y705, Cell Signaling Technologies
246 #D4XC3), STAT3 (D3Z2G, Cell Signaling Technologies #63585), pAKT (S473, Cell Signaling
247 Technologies #4060), AKT (11 E 7,Cell Signaling Technologies #4685), pERK (T202/Y204,Cell
248 Signaling Technologies #4370S), ERK2 (137F5, Cell Signaling Technologies #4695), CA2
249 (EPR5195,Abcam #ab124687), SPINK1 (CGQG032302A R&D #AF7496), and Cofilin (D3F9, Cell
250 Signaling Technologies #5175). Secondary antibodies used were Peroxidase AffiniPure™ Goat
251 Anti-Mouse IgG (H+L) (Jackson ImmunoResearch #115-035-003), Peroxidase AffiniPure™
252 Donkey Anti-Rabbit IgG (H+L) (Jackson ImmunoResearch #711-035-152), Peroxidase
253 AffiniPure™ Goat Anti-Rabbit IgG (H+L) (Jackson ImmunoResearch #111-035-003), Sheep IgG
254 Horseradish Peroxidase-conjugated Antibody (R&D Systems #HAF016), IRDye 800 CW Goat
255 Anti-Rabbit IgG (Licor Bio #926-32211) and IRDye 680 CW Goat Anti-Mouse IgG (Licor Bio #926-
256 68070).
257
258 hCP35 and hCP44 organoids at 50-70% confluency were treated with Ivacaftor (3 μM-
259 MedChemExpress #HY-13017), combination of Ivacaftor, Elexacaftor (3 μM -MedChemExpress
260 #HY 111772), and Tezacaftor (3 μM- Selleck Chemicals #S7059), or vehicle control for 48 hours
261 in human complete feeding media prior to whole cell lysate collection, as described above.
262
263 Western blots were developed using either a film processor (Mini-Med 90- AFP Manufacturing
264 Corporation) or Odyssey M (LiCor). Quantification of immunoblots was conducted using either
265 ImageJ or Empiria Studio.
266
267 *WGS library preparation, sequencing, variant calling, and primary tissue- organoid SNP*
268 *concordance*
269

DNA was isolated from PDOs after at least 3 passages. Isolation of primary tissue DNA was conducted from flash frozen or viably cryopreserved samples. Genomic DNA was isolated from organoids or primary tissue using DNeasy Blood and Tissue Kit (Qiagen #69504). WGS libraries were prepared using Nextera XT (Illumina DNA library) in accordance with the manufacturer's instructions. Final libraries were evaluated using TapeStation (Agilent). Libraries were sequenced on an Illumina NovaSeq X sequencer for 30 x coverage for primary tissues and PDO.

Raw data was aligned to the hg38 reference genome with bwa mem v0.7.12-r1039. PCR duplicates were marked with Picard v1.130, and germline variants were called with GATK's haplotypecaller, v4.0.8.1. SNPs and INDELs were filtered with vcftools v0.1.13 the parameters: max-missing=0.5, mac=2, min-meanDP=15, minQ=32. For the purposes of concordance testing, multi-allelic sites and sites with missing genotype calls were discarded.

Concordance was determined using R 'irr' package (version 0.84.1) using intraclass correlation coefficient (ICC) using a two-way model with a 0.95 confidence level. As a control, comparison of PDOs from two different patients and found a match rate of 72% with an ICC of 0.4. When comparing a PDO from one patient to the primary tissue of another, the match rate is 74% with an ICC of 0.43.

Germline pathogenic variants were investigated in: ABCG8, APOA5, APOB, CASR, CFTR, CLDN2, CTRC, GGT1, HLA-DQA1, HLA-DQB1, LPL, PRSS1, PRSS1-PRSS2, SLC10A2, SLC26A9 and SPINK1

RNA isolation and RNA-seq library construction

For RNA-seq experiment, organoids in Matrigel were lysed directly with 1 mL of TRIzol reagent (Thermo Fischer #15596018), and total RNA was extracted using RNeasy Mini Kit (Qiagen #74104). RNA quality control was performed on all samples using Qubit Fluorometer (Invitrogen) and TapeStation (Agilent) before RNA-seq analyses. A total of 200 ng of high-quality RNA (RIN > 8, assessed by Agilent TapeStation) was used for library construction. mRNA was enriched using poly(A) selection, followed by fragmentation. First- and second-strand cDNA synthesis was performed, and 3′ adenylation was carried out prior to ligation of Illumina-compatible adapters containing unique dual barcodes. Adapter-ligated fragments were enriched by limited-cycle PCR amplification. Final libraries were assessed for quality and fragment size distribution using the Agilent Bioanalyzer DNA 1000 kit, and equal amounts of libraries were pooled for sequencing on an Illumina platform. Novaseq 6000 sp reagent kit v 1.5 was used to sequence samples for 300 cycles for 150 bp paired end reads using an Illumina Novoseq 6000.

snRNA-seq analysis, RNA-seq analysis, PCA visualization, and differential gene expression analysis

Raw reads were quality checked with FASTQC (v0.12.1)[57]. Poor quality 3' ends and sequencing adapters were trimmed with Cutadapt (v4.9)[58] and reads shorter than 20nt were filtered. Trimmed reads were again checked with FASTQC, then aligned to human reference genome (hg38 from UCSC with gene annotation gencode.v45.basic.annotation.gtf)[59,60] and genes quantified with STAR[61] (2.7.11b). Subsequent analysis was performed in R (version shown below, R Core Team 2024).

The column with 2nd read strand aligned with RNA from the STAR generated expression tables were used since the library prep was strand specific. Expressions were normalized with DESeq2[62] and the top 500 most variable genes after variance stabilization were used for the PCA plot and

heatmap. DESeq2 was also used for differential gene analysis, with cutoffs padj <0.05 and $|\log_2 \text{FoldChange}|$ >1. These values plotted in the volcano plot for every gene.

Nonnegative matrix factorization exclusively for hCP was performed with the NMF library[63,64]. Ranks 2 through 7 were tested, each with 500 runs to determine the optimal rank. Based on consensus throughout 500 runs, as well as the rank survey scores from the best run each rank, rank 3 was picked as the optimal rank. The consensus shows the best run from the 500 and which samples clustered together but basis was the parameter used to determine the most stable subtypes. Differential gene analysis was performed again, this time separated by basis found with NMF.

Normalized counts from DESeq2 were analyzed with GSEA comparing either hCP with hNAT and hNP, or between hCP bases to determine enriched gene sets[65,66]. GSEA was also used to find gene markers specific to ductal or acinar samples from BioProject PRJNA924346[67]. Each individual PDO transcriptome profile was projected onto the set of ductal or acinar gene markers by single sample GSEA to assess their similarity[68] .

Tumor PDO sample transcriptomes were obtained from NCBI dbGAP accession phs001611.v1.p1[43]. Differentially expressed genes with padj < 0.05 from tumor (hT) vs. normal, and hCP vs hNP and hNAT were integrated to find concordant or discordant expression patterns.

Heatmaps are generated with pheatmap or Graphpad Prism, all other figures are generated with ggplot2. R version and library versions are below.

EGAC00001001732 snRNA-seq data was analyzed[69], and the ductal cell cluster was interrogated. CP ductal cells contained 903 nuclei from 1 male and 1 female CP patient with unknown etiology, who are 71 and 52 years of age, respectively. NP ductal cells contained 4,432 nuclei from 3 NAT patients (2 female, 1 male, 46, 59, and 77 years of age respectively).

Fluorescent in situ hybridization

Sections were formalin fix and paraffin embedded. Reagents for the RNAscope Multiplex Fluorescent Reagent kit V2 (#323280) along with RNAscope 4-plex Ancillary Kit for Multiplex Fluorescent Reagent kit V2 (#323120) from Advanced Cell Diagnostics (Newark, CA, USA) were used in accordance with the manufacturer's instructions using the HybEZ Hybridization system (#241000). Probes were all designed by Advanced Cell Diagnostics: *Gpx3* (#470591-C3), *Aqp1* (#421831-C2), *Bpifb1* (#576511-C4). We used the manual target retrieval method described in appendix B of the protocol for 15 minutes with protease plus treatment for 15 minutes. Fluorescent dyes used TSA Vivid fluorophore 520 (323271- 1:3000), 570 (323272- 1:3000), 650 (323273-1:3000), and Opal 780 (# FP1501001KT- Akoya Biosciences; Opal TSA-DIG 1:3000; Opal Polaris 780 1:750). Sections were counterstained with DAPI, sealed with a coverslip using ProLong Gold Antifade reagent (Invitrogen #P36930), and then dried overnight covered from light. Imaged using either Fluoview FV 3000 confocal microscope at 30x or whole slide Zeiss Axioscan 7 at 20x.

Forskolin induced swelling assay

Organoids were seeded into 96-well clear bottom plates in 8 µL domes at a confluency between 50-70%. Organoids were fed human complete medium after seeding. 18-12 hours prior to treatments, media was changed and PGE_2 was removed from media. For dependency studies, organoids were treated with CFTR and PKA inhibitors for 2 hours prior to forskolin administration

(10 μM CFTRinh-172- Selleck Chemicals #S7139; 5 μM PPQ-102- Selleck Chemicals #S1565; 20 μM H-89- Fisher #501873404; 20 μM forskolin- Selleck Chemicals #S2449). Restoration of CFTR function was investigated using CFTR potentiators (10 μM Icenticaftor (QBW251)- Selleck Chemicals #S9973; 10 μM Ivacaftor- MedChemExpress #HY-13017; 10 μM Ivacaftor- Selleck Chemicals #S1144), CFTR corrector (10 μM Lumacaftor- Selleck Chemicals #S1565; 10 μM Elexacaftor- MedChemExpress #HY 111772, Selleck Chemicals #S8851; 10 μM Tezacaftor- Selleck Chemicals #S7059). Mouse normal organoids treated with 20 μM forskolin were used as a positive control for assay. All compounds were dispensed using a Tecan HP D300e in DMSO. Organoids were imaged using brightfield imaging on a Tecan Spark Cyto. Images were taken at time of treatment and 6 hours post treatment with CFTR correctors, potentiators, or forskolin. The area of 10 organoids was measured at these two time points using either QuPath 0.5.0 or ImageJ. The relative area at 6 hours was used for comparison across treatment groups. T-tests and ANOVA statistical tests were conducted.

Data visualization

Data was visualized using R studio (2024.04.2+764) and GraphPad Prism (9 & 10). Figures were arranged in Adobe Illustrator.

Data Availability

Raw data for whole genome sequencing and RNA-seq will be publicly available on NCBI the database of genotype and phenotypes (dbGAP) upon final publication of manuscript.

397 **Results**
398
399 *Generation of organoids from patients with human chronic pancreatitis (CP) with high efficiency*
400
401 We received 51 CP surgical specimens (**Table 1, S1, Figures 1A-B, S1A-C, S2A-B**). The
402 patient cohort was predominantly female (65%), with a mean age of 38 years. The mean age was
403 45 years for patients with idiopathic CP, 25 years for genetic CP, and 47 years for alcohol-related
404 CP. Most patients self-identified as white and non-Hispanic. Idiopathic CP was the most common
405 diagnosis, accounting for 41% of the cohort (**Figure 1B**). Among the 51 patient specimens
406 received, 24 were from patients who underwent genetic testing. Pathogenic variants were
407 reported in CFTR (20%, n=10), PRSS1 (14%, n=7), and SPINK1 (12%, n=6) (**Figure 1C**).
408 Most CP specimens were obtained following total pancreatectomy islet auto
409 transplantation (TPIAT, 75%), and the remainder were from partial pancreatectomies (25%)
410 (**Figures 1B, S1A-C, Table S1**). Pancreatectomy specimens were obtained within 2 hours post-
411 resection with intact parenchyma but were often heavily cauterized (**Figure S1B-hCP1, hCP3,**
412 **S1C- hCP10)**. TPIAT specimens were partially dissociated and then received typically 24-48
413 hours post-surgery, often with disrupted parenchyma. When sufficient intact tissue was available,
414 a portion of the specimens were fixed for histology (**Figures 1A, S1A**). Histologic assessment of
415 the primary specimens by a pathologist confirmed classic CP features, including parenchymal
416 atrophy, fibrosis, and ductal abnormalities (**Table 1, S1, Figures 1A, S2A-B**). Fibrosis scoring
417 and quantification of collagen deposition revealed substantial desmoplasia, with some specimens
418 containing little to no remaining acinar epithelial tissues (**Table 1, S1, Figures 1B, S2A-B**).
419 Organoids were observed after 1-7 days in culture and could be passaged every 4-7 days,
420 12-25 times, similar to the passaging potential of normal pancreas (NP) organoids (**Figure S1D-**
421 **E**). PDO generation efficiency was determined after 5 passages to exclude lines that did not
422 expand. Generation of 3 PDO lines are still in process and have not yet reached 5 passages. Out
423 of the 48 specimens that have reached evaluation criteria, 36 yielded PDO lines. We successfully
424 generated organoids from 70% of CP specimens (**Table 1, Figure 1D**). Failures occurred due to
425 a lack of viable epithelial cells when tissue was frozen upon arrival, extensively cauterized, or
426 composed primarily of fibrosis (**Figure S2B, Table S1**). PDO generation efficiency was higher for
427 TPIAT specimens (77%) relative to partial pancreatectomy samples (56%) (**Figure 1D**).
428 CP organoids displayed a consistent, homogenous cystic morphology with a single cell
429 layer (**Figure 1E**). Organoid morphology, passage time, and passaging potential did not differ
430 across CP etiologies (**Figure S1D-E**). CP PDOs are comprised of rapidly dividing ductal epithelial
431 cells as demonstrated by incorporation of EdU and immunofluorescence (IF) for CK19 (**Figure**
432 **1F-G, S1F**).
433
434 *PDOs have high genetic concordance and reveal important and previously unannotated*
435 *alterations*
436
437 We assessed the genetic fidelity of PDOs by performing genomic analyses on matched
438 primary and PDO specimens. Genomic alterations were compared between PDOs and primary
439 tissue by whole genome sequencing (WGS), whole exome sequencing (WES), or targeted
440 sequencing (**Figures 2, S3A, Table S1**). More than 9 million single nucleotide polymorphisms
441 (SNPs) and almost 2 million insertions and deletions (indels) were compared by WGS, revealing
442 an average 98% match rate with an intra correlation coefficient (ICC) of 0.96 between 14 pairs of
443 PDOs and primary tissue (**Figures 2, S3A**). More than 80,000 SNPs and 7,000 indels were
444 compared by WES, revealing an average 91% match rate with ICC of 0.83 between 6 pairs of
445 PDOs and primary tissue (**Figures 2**, denoted by # in **S3A**). These data demonstrate the high
446 genetic concordance between patient-matched primary tissue and PDOs. NP PDOs did not

447 contain any pancreatitis-associated pathogenic mutations nor PDA-associated oncogenic
448 alterations.
449 We then queried germline variants in 14 genes associated with hereditary pancreatitis. All
450 clinically annotated PRSS1, SPINK1, and CFTR germline variants are retained in our PDOs
451 (**Figure 2**). PRSS1 has five paralogs with 90-91% nucleotide similarity, resulting in reads aligning
452 to multiple locations with low mapping quality scores (MapQ)[70,71]. The PRSS1 N91I mutation was
453 called with high confidence (hCP49), while the R122H (hCP24, hCP35) and R116C mutations
454 (hCP49) were identified with low MapQ scores (**Figure 2**). Mutations in SPINK1 were confirmed
455 in both PDO and pancreatic tissue from hCP08, hCP11, hCP30, hCP36, and hCP49. Interestingly,
456 in 2 PDOs from patients with idiopathic CP with no previous genetic testing, we found SPINK1
457 N34S mutation (hCP07, hCP48) (**Figure 2**). In addition, we identified an unannotated SPINK1
458 P55S mutation (hCP35) and LPL N318S mutation (hCP32), which is associated with
459 hyperlipidemia[72] and hereditary CP[73] (**Figure 2**).
460 Intronic variants of CFTR are common[30] and were confirmed in agreement with patient
461 genetic testing results (hCP25, hCP28, and hCP32) (**Figure 2**). 9T variants are included in our
462 assessment because their impact on exon 9 skipping in the pancreas in unknown despite minimal
463 effect in nasal epithelium[74]. We confirmed the PDOs recapitulate coding sequence variants of
464 CFTR, including R75Q, R117H, E217G, R347P, W1282*, and Q1352H mutations (**Figure 2**)[75-81].
465 Additionally, 75% of the CP PDO cohort harbors the CFTR V470M variant, which has conflicting
466 reports of pathogenicity in association with CP and is likely a passenger mutation[75,80-84]. Additional
467 G576A and R668C CFTR mutations were detected in hCP07, which have been found to be co-
468 mutated in hereditary pancreatitis[85-87]. Also, a mild V201M CFTR variant was found in hCP32[88].
469 CFTR mutations associated with hereditary CP are distinct from cystic fibrosis and often do not
470 overlap[25-32]. None of the cystic fibrosis associated CFTR mutations (CFTR2 database, n=1092)
471 are found in the CP PDO cohort (**Figure S3B**).
472 Importantly, CP is a risk factor for developing pancreatic cancer and some hereditary CP
473 patients have up to a 55% lifetime risk. The PDO platform enables identification of potential
474 somatic oncogenic variants that are present in a small percentage of epithelial cells that would be
475 obscured by the low epithelial cellularity of primary tissues. Here, we identified oncogenic KRAS
476 G12D mutation in hCP30 with an allele frequency of 0.21 that was not detected in the primary
477 specimen. We also found oncogenic TP53 R175H mutation in hCP28 at an allele frequency of
478 0.05 that was not detected in the primary specimen. These data suggest that the CP PDO models
479 may be useful in identifying patients at higher risk of progressing to PDA.
480
481 *Gene expression analyses demonstrate distinct cell signaling programs in CP organoids*
482 To understand the specific programs differentially regulated in CP PDOs, we performed
483 RNA-seq on 24 CP, 9 NP, and 4 normal adjacent to tumor (NAT) PDOs. Ductal lineage identity
484 is maintained by all PDOs with no evidence of non-epithelial cell contamination (**Figure S3C**),
485 concordant with positivity for the ductal epithelial marker CK19 by IF (**Fig. 1F**). CP PDOs have a
486 distinct transcriptomic profile as compared to NP and NAT PDOs (**Figures 3A-C**). Gene set
487 enrichment analyses (GSEA) reveal that CP PDOs are enriched in gene sets associated with
488 inflammatory response, TNFA signaling via NFKB, KRAS signaling, Epithelial to Mesenchymal
489 Transition (EMT), and TGF beta signaling while having depressed Oxidative Phosphorylation
490 relative to NP and NAT PDOs (**Figure 3D**). Compared to NP and NAT PDOs, CP expressed
491 higher levels of fibrosis and inflammatory cytokine associated genes (e.g., *COL1A1*, *TGFB2*,
492 *IL1A*, *CSF1*) (**Figure 3E**), suggesting that CP PDOs maintain the fibrosis and inflammatory
493 programs present in CP patients[89].
494 Principal component analysis of CP PDOs suggested the presence of 3 distinct clusters
495 (**Figure S4A**). The PDO transcriptomes were independently clustered using nonnegative matrix
496 factorization (NMF)[63,64], revealing 3 stable subtypes in CP PDO cultures (basis 1-3) (**Figures 3F**,

497 **S4B**). The molecular subtypes identified using this approach do not cluster according to etiology
498 (**Figure 3F**), suggesting distinct subtypes independent of TIGAR-O classification. We performed
499 GSEA on each CP subtype relative to NP and NAT PDOs (**Figure S4C**). The basis 1 subtype is
500 depleted in oxidative phosphorylation and enriched in EMT and apoptosis gene sets. The
501 apoptosis gene set includes proteins that involve cellular stress response pathways, such as
502 glutathione peroxidase 3 (GPX3). The basis 2 subtype is enriched in E2F targets, MYC targets,
503 and myogenesis. The basis 3 subtype is enriched in E2F targets. All subtypes trend towards
504 enrichment of the inflammatory response gene set.
505 To validate these subtypes in matched primary tissue specimens, we identified the genes
506 that were differentially expressed between the 3 subtypes of CP and have the highest Kim-score,
507 and therefore drive these distinct clusters (**Figure S4D**). Subtype defining genes were evaluated
508 by RNA *in situ* hybridization (**Figure S5A**). We found that a patient specimen from the basis 1
509 subtype PDO hCP1 expressed the highest levels of GPX3 as expected. The patient matched
510 specimen for the basis 2 subtype PDO hCP3 exhibited the highest level of aquaporin 1 (AQP1*)*.
511 The basis 3 subtype was defined by BPI-family member B 1 (BPIFB1*)*, which exhibited the highest
512 levels in patient specimen from the basis 3 subtype PDO hCP48. This indicates that the genes
513 driving CP PDO transcriptional subtypes can also be detected in the corresponding primary
514 tissue.
515 Transcriptomic analyses on primary CP tissues are challenging due to the high degree of
516 fibrosis and the high levels of RNases. We further explored the expression of subtype-defining
517 genes using single-nucleus RNA sequencing (snRNA-seq) data from human NAT and CP
518 samples[69]. In the ductal cell cluster, we observed that subtype defining genes were expressed in
519 primary pancreatic ductal epithelium (**Figure S5B-C**), but insufficient sample and cell numbers
520 made identification of subtypes in these data challenging. These findings confirm that the genes
521 driving transcriptional subtypes in the CP PDOs are present in an independent patient cohort.
522 Additional analysis comparing the transcriptomes of our CP PDO cohort to human
523 pancreatic cancer organoids revealed genes that are uniquely expressed in either disease
524 (**Figure S5D**). This along with the discovery of somatic oncogenic variants in 2 of our CP PDOs
525 demonstrate that this model can be used to study patients with heightened risk of cancer and to
526 identify early detection biomarkers.
527
528 *CP organoids recapitulate protein expression from primary tissue specimens and exhibit elevated*
529 *inflammatory and mitogenic signaling*

530 Immunohistochemistry (IHC) and immunoblotting (IB) were used to evaluate proteins and
531 glycan levels associated with pancreatitis, as well as mitogenic and inflammatory signaling. CP
532 and NP PDOs exhibited protein alterations consistent with matched patient specimens (**Figures**
533 **4A-B**). We previously found that up to ~90% of adult CP has local elevation of CA19-9[90]. Patient
534 specimens had a range of CA19-9 that matched CP PDOs (**Figures 4A-B**). Activation of EGFR
535 has been reported in human CP[91]. A subset of CP PDOs have elevated levels of phospho-EGFR
536 and downstream effectors AKT and ERK relative to NP PDOs (**Figure 4A**), suggesting there are
537 "mitogenic" and "non-mitogenic" CP subtypes. NP PDOs primarily express mature CFTR by IB
538 (upper band, C-band, 150-160KD[92]) with very little immature CFTR (lower band, B-band, 135-
539 140KD[92]) (**Figures 4A, S6A**). Of those with CFTR mutations, hCP11 and hCP44 had low levels
540 of mature CFTR by IB, which was replicated in the primary patient specimen IHC (**Figures 4A-**
541 **B**). This corresponds with what is known about the pre-mature stop codon mutation present in
542 hCP11 and compound CFTR R347P; R117H mutation in hCP44. These mutations have been
543 reported to lead to major folding defects, and thus, as expected, do not produce mature CFTR[79].
544 E217G and R75Q CFTR mutations found in hCP08 and hCP17, respectively, impact anion
545 channel function[75,92], but not protein maturation. These two lines have mature CFTR, as predicted.
546 hCP15, a non-hereditary case attributed to alcohol and hypothyroidism, also demonstrated loss

547 of mature CFTR protein despite having a benign V470M mutation (data not shown). Decreased
548 CFTR expression and function has been shown to occur secondary to alcohol[93,94], tobacco[95], and
549 hypothyroidism[96]. These findings suggest that CFTR modulators that increase protein activity may
550 help even CP patients without pathogenic CFTR mutations. Carbonic anhydrase 2 (CA2), which
551 catalyzes the conversion of CO_2 into HCO_3^-, was decreased in most CP PDOs when compared
552 to NP, pointing to another possible mechanism through which HCO_3^- secretion may be impaired
553 in CP (**Figure 4A**).
554 To identify fibroinflammatory mediators in CP PDOs at the protein level, we evaluated
555 conditioned medium from 14 CP and 9 NP PDOs. IL1A, TGFB2, CX3CL1, and other
556 fibroinflammatory secreted factors were elevated in CP PDOs and reflected the changes
557 observed in gene expression and published changes in CP patients[97,98] (**Figure 4C, S6B**),
558 demonstrating the ability of CP PDOs to model inflammatory changes seen in patients. Together,
559 these data support that PDOs retain key molecular features of CP, including alterations in cell
560 signaling proteins.
561
562 *CFTR function in CP organoids is restored upon pharmacologic modulation*

563 The forskolin-induced swelling (FIS) assay was developed to measure CFTR dysfunction
564 and previously deployed in intestinal and rectal organoids from cystic fibrosis patients to predict
565 response to CFTR modulators[39,40]. Intestinal current measurements and FIS activity were tightly
566 correlated, demonstrating that FIS assays can serve as a surrogate for more complex
567 electrophysiological measurements[40]. We optimized the FIS assay in murine and human NP
568 PDOs (**Figure 5A**). Vehicle treated organoids had no response, but forskolin or CFTR potentiator
569 treatment caused organoid swelling (**Figures 5B-F, S7A-C**). Swelling was inhibited when mouse
570 and human NP organoids were treated with CFTR inhibitors (CFTRi-172, PPQ-102) or a PKA
571 inhibitor (H-89), demonstrating that swelling is dependent on forskolin induced activation of CFTR
572 via PKA (**Figures 5D-F, S7B**). Mouse normal organoids served as a positive control while testing
573 the CFTR function of CP PDOs (**Figure S7A-B)**. Half of the CP PDOs evaluated (n=4 out of 8)
574 were FIS impaired across multiple experimental replicates (**Figure 5G**, **S7D**).
575 Most CFTR wild type PDOs (hCP1, hCP3, hCP48, hCP49) swelled in response to forskolin
576 treatment as expected (**Figure 5G**). Unexpectedly, hCP16, which is CFTR wildtype and exhibits
577 normal CFTR protein levels (**Figure 4A**), is FIS deficient (**Figure 5G, S7D**). We hypothesized that
578 organoids deficient in FIS could be rescued by treatment with CFTR potentiators, which increase
579 the basal activity of CFTR (**Figure 6A**). Treatment of hCP16 with CFTR potentiators did not
580 restore swelling (**Figure S7D**), suggesting that the dysfunction in FIS in this PDO is independent
581 of CFTR.
582 hCP11 did not swell, which can be attributed to the lack of mature CFTR due to a
583 premature stop codon mutation (**Figures 4A**)[99]. Given the lack of mature CFTR protein, treatment
584 with CFTR potentiators did not restore swelling (**Figure 6B**). However, treatment with the read
585 through agent, Ataluren, was able to restore FIS response (**Figure 6C**) and increase levels of
586 mature CFTR (**Figure 6D**). These data demonstrate that we can successfully achieve genotype-
587 driven precision therapeutics in CP PDOs.
588 hCP35 is CFTR wildtype and exhibits normal CFTR protein levels. Unexpectedly, hCP35
589 had a limited FIS response (**Figures 5G, 6E**). Swelling was restored by treatment with CFTR
590 potentiators, Ivacaftor and Icenticaftor (**Figure 6E**). This demonstrates ability of potentiators to
591 increase CFTR function in PDOs even with wild type CFTR.
592 hCP44 was also deficient in FIS (**Figure 6F, 6I**), which was expected given the CFTR
593 R347P, R117H mutations that impair protein folding and anion transport[100] and because the low
594 levels of mature CFTR protein (**Figure 4A**). The protein folding defect can be ameliorated with
595 CFTR correctors. This class of drugs increases the correct folding and plasma membrane
596 localization of CFTR and the combination of correctors and potentiators is FDA approved for the

treatment of cystic fibrosis (e.g., Orkambi: Ivacaftor, Lumacaftor)[101]. hCP44 FIS was rescued by treatment with a combination of correctors and potentiators (Orakambi, and Ivacaftor + Elexacaftor) (**Figure 6G**), but not monotherapies (**Figure 6F**). This demonstrates that CP PDO models can used to identify the most effective combinatorial treatment strategies in the background of complex allelic combinations.

We tested if treatment with CFTR correctors and potentiators increases mature CFTR protein levels in FIS deficient hCP35 and hCP44. Single agent treatment of hCP35 with the potentiator Ivacaftor marginally increased mature CFTR, which was further increased by ETI treatment (**Figure 6H**). As expected from our FIS results, ETI treatment increases mature CFTR protein levels in hCP44 (**Figure 6I**). Importantly, treatment of hCP44 with single agent CFTR potentiator caused a decrease in mature CFTR protein levels (**Figure 6I**). This is in line with previous findings that Ivacaftor treatment can interfere with CFTR stability in the background of certain mutations, such as the R347P, R117H alterations found in hCP44[102]. These findings stress the importance of investigating CFTR modulator response in patient-specific contexts, especially in the setting of complex allelic combinations. Altogether these data indicate that patients with and without pathogenic *CFTR* alterations could benefit from ETI treatment to increase mature CFTR expression. Treatment with ETI in both hCP35 and hCP44 also led to a decrease in pERK and pSTAT3 levels (**Figures 6H-I**), suggesting that restoration of CFTR function can decrease mitogenic and inflammatory signaling. Our findings suggest that restoring normal ductal function can contribute to the resolution of inflammation.

Discussion

Surgical samples from chronic pancreatitis patients are rare, making this CP PDO biobank a unique resource. Importantly, while our PDO biobank encompasses the major etiologies of CP, the patients are a highly selected cohort that required surgical management. In the future, this limitation may be addressed through generation of CP PDOs from pancreatic juice, which we accomplished in 2 cases and is a more accessible sample source.

The identification of pathogenic germline alterations in 3 patients diagnosed with idiopathic CP suggests that genetic testing may have broader benefit in CP clinical care. Two of the CP PDOs also contain oncogenic mutations in TP53 or KRAS, known drivers of pancreatic ductal adenocarcinoma. This is expected given the high rate of sporadic KRAS mutations that have been found in autopsy studies of the normal human pancreas[103]. Work has also shown that even in the context of wild type KRAS, TP53 mutation promotes injury in a non-cancer context[104]. CP PDO models will facilitate our understanding of which patients are at risk of severe disease and progression to PDA. Identification of the KRAS and TP53 mutations were uniquely possible from analysis of the PDOs and not the tissue. Further work is needed to explore how CP PDOs can be leveraged to model the transition from a chronic inflammatory state to invasive carcinoma.

CP is primarily classified by etiology, but our transcriptomic analyses reveal molecular subtypes that do not correlate with etiology, suggesting that distinct cell signaling changes drive CP subtypes. The validation of these subtypes remains challenging due to the limited availability of these surgical tissue specimens and the high abundance of RNases and proteases in the pancreas. Future work will focus on creating primary CP specimen data resources for corroboration of these findings and for investigation of clinical correlates. These subtypes offer an initial framework to explore potential signaling pathways driving CP pathogenesis.

Surprisingly, the CP PDOs maintain a fibroinflammatory gene and protein expression signature despite being removed from the microenvironment. These data suggest that ductal cells can contribute to maintenance of the fibroinflammatory program and opens several lines of questioning. When are these ductal gene expression programs established and how are they maintained? Is the intrinsic epithelial fibroinflammatory program sufficient to cause CP and promote PDA initiation? Would reversing this program restore pancreatic function? CP PDOs

647 enable exploration of these important questions at unprecedented depth as well as the
648 appropriate physiologic context.
649 The use of PDOs for functional precision medicine has been previously established in
650 pancreas cancer[43,46,50,52]. Here, we show that CP PDOs can be similarly used as a platform for
651 studying CFTR function in different complex genetic contexts and delineating treatment response.
652 Our study shows that CP PDOs are commonly deficient in FIS. This deficiency can be effectively
653 reversed by treatment with FDA-approved CFTR modulators, suggesting potential targeted
654 therapeutic strategies for the treatment of CFTR-mutant CP. An important consideration when
655 testing CFTR modulators to treat CP includes organ context and species. CFTR mutations in
656 cystic fibrosis patients primarily impacts chloride secretion whereas in the pancreas, it contributes
657 substantially to bicarbonate transport. This highlights the importance of investigating CP CFTR
658 mutations in pancreatic cell types. In addition, mutant mouse CFTR does not respond to human
659 CFTR modulators[41]. This is further complicated by reduced levels of bicarbonate in mouse
660 pancreatic juice (50 mM) relative to human (140 mM)[37], suggesting a lower level of reliance on
661 bicarbonate in the mouse pancreas. Finally, as evidenced in our cohort, the genetics of CP is
662 complex. There are more than 2,000 different CFTR mutations and limited information regarding
663 drug response to most of these alterations, especially those associated with hereditary CP. Even
664 in the setting of the same pathogenic alterations, patient response to CFTR modulators is very
665 heterogeneous, highlighting the need for precision medicine approaches[35-40]. The physiologically
666 relevant context of human CP PDOs enables direct investigation of genotypic relationships to
667 therapeutic responses. We further demonstrate CFTR dysfunction in CP PDOs with wildtype
668 CFTR that can be restored with potentiator treatment, raising the possibility that this treatment
669 approach could be widely applicable to a large patient population. Our work also highlights the
670 utility of restoring normal homeostatic function to reduce inflammatory signaling as evidenced by
671 decreased STAT3 activation following CFTR modulator treatment. Altogether, we demonstrate
672 the power of our PDO platform to study the underlying molecular pathogenesis of human CP and
673 pave the way for precision therapeutics.

674 **Acknowledgements**
675 The authors would like to extend our deepest gratitude to all the patients who generously
676 consented to participate in this study. The authors would like to thank all the members of the
677 Engle laboratory, the UCSD Biorepository and Tissue Technology Shared Resource (BTTSR),
678 the UCSD Department of Surgery, the University of Minnesota Departments of Surgery and
679 Pediatrics, April Williams, Ling Ouyang, and Tzu-when Wang at the NGS Core Facility of the Salk
680 Institute, Elsa Molina at the Single-Cell and Spatial Omics core of the Salk Institute, Daniela
681 Boassa, Sammy Weiser Novak and Elsie Quansah at the Biophotonics Core Facility of the Salk
682 Institute, and the Lifesharing Donate Life organization.
683
684 **Funding Statement**
685 V.O.V is supported through the Salk Institute Cancer Training Grant (T32CA009370). J.C.L. was
686 supported through the Salk Institute Cancer Training Grant (T32CA0093790). This work was
687 supported by the Razavi Newman Integrative Genomics and Bioinformatics Core Facility of the
688 Salk Institute with funding from NIH-NCI CCSG: P30 CA01495, NIH-NIA San Diego Nathan Shock
689 Center P30 AG068635, and the Helmsley Trust. This work was supported by the Waitt Advanced
690 Biophotonics Core Facility of the Salk Institute with funding from NIH-NCI CCSG: P30 CA01495,
691 NIH-NIA San Diego Nathan Shock Center P30 AG068635, and the Waitt Foundation. This work
692 was supported by the NGS Core Facility of the Salk Institute with funding from NIH-NCI CCSG:
693 P30 CA01495, NIH-NIA San Diego Nathan Shock Center P30 AG068635, the Chapman
694 Foundation and the Helmsley Charitable Trust. The Biorepository and Tissue Technology Shared
695 Resource is supported by a National Cancer Institute Cancer Center Support Grant (CCSG
696 P30CA23100) and by recharges from users. This research program was supported by Mission

Cure Capital, LLC, the Lustgarten Foundation, the Conrad Prebys Foundation, The Paul M. Angell Family Foundation, Curebound (20DG11), and by the Helen McLoraine Developmental Chair.

Land Acknowledgement

The Salk community holds great respect for the land and the original people of the area where our campus is located. The Institute is built on the territory of the Kumeyaay Nation. Today, the Kumeyaay people continue to maintain their political sovereignty and cultural traditions as vital members of the San Diego community. We acknowledge their tremendous contributions to our region and thank them for their stewardship.

Declaration of Interests

J. Gibson, and D. Whitcomb are founders of Ariel Precision Medicine. D. Whitcomb is a member of its scientific advisory board at Ariel Precision Medicine. P. Greer is an employee of Ariel Precision Medicine.

References

1. Kleeff, J., Whitcomb, D.C., Shimosegawa, T., Esposito, I., Lerch, M.M., Gress, T., Mayerle, J., Drewes, A.M., Rebours, V., Akisik, F., et al. (2017). Chronic pancreatitis. Nature Reviews Disease Primers *3*, 17060. 10.1038/nrdp.2017.60.
2. ZM, S., D, M., H, Y., M, D., KY, Z., R, B., JJ, W., C, K., and KT, P. (2018 Aug). Nationwide Trends in Acute and Chronic Pancreatitis Among Privately Insured Children and Non-Elderly Adults in the United States, 2007-2014 - PubMed. Gastroenterology *155*. 10.1053/j.gastro.2018.04.013.
3. Jorge D Machicado (1), V.R., Dhiraj Yadav (1) (28/07/2016). Epidemiology of Chronic Pancreatitis. Pancreapedia: The Exocrine Pancreas Knowledge Base. 10.3998/panc.2016.13.
4. Whitcomb, D.C., and Group, N.A.P.S. (2019). Pancreatitis: TIGAR-O Version 2 Risk/Etiology Checklist With Topic Reviews, Updates, and Use Primers. Clinical and Translational Gastroenterology *10*, e00027. 10.14309/ctg.0000000000000027.
5. Vege, S.S., and Chari, S.T. (2022). Chronic Pancreatitis. New England Journal of Medicine *386*, 869-878. 10.1056/nejmcp1809396.
6. JS, T., L, K., U, B., and M, G. (03/23/2009). Smoking and risk of acute and chronic pancreatitis among women and men: a population-based cohort study - PubMed. Archives of internal medicine *169*. 10.1001/archinternmed.2008.601.
7. Yan, M.-X., and Li, Y.-Q. (2006/04/01). Gall stones and chronic pancreatitis: the black box in between. Postgraduate Medical Journal *82*. 10.1136/pgmj.2005.037192.
8. Otsuki, M., and Otsuki, M. (2003/04). Chronic pancreatitis in Japan: epidemiology, prognosis, diagnostic criteria, and future problems. Journal of Gastroenterology 2003 38:4 *38*. 10.1007/s005350300058.
9. Yadav, D., Whitcomb, D.C., Yadav, D., and Whitcomb, D.C. (2010-02-02). The role of alcohol and smoking in pancreatitis. Nature Reviews Gastroenterology & Hepatology 2010 7:3 *7*. 10.1038/nrgastro.2010.6.
10. Singh, V.K., Yadav, D., and Garg, P.K. (2019). Diagnosis and Management of Chronic Pancreatitis. JAMA *322*, 2422-2434. 10.1001/jama.2019.19411.
11. AE, P., J, L., P, G., J, A., S, A., ST, A., MA, A., J, B., PA, B., RE, B., et al. (2018 Jul). Known genetic susceptibility factors for chronic pancreatitis in patients of European ancestry are rare in patients of African ancestry - PubMed. Pancreatology : official journal of the International Association of Pancreatology (IAP) ... [et al.] *18*. 10.1016/j.pan.2018.05.482.
12. J, C., R, L., DI, W., A, C., and R, C. (07/03/1999). Mutations of the cationic trypsinogen gene in patients with chronic pancreatitis - PubMed. Lancet (London, England) *354*. 10.1016/S0140-6736(99)01814-0.
13. Schwarzenberg, S.J., Uc, A., Zimmerman, B., Wilschanski, M., Wilcox, C.M., Whitcomb, D.C., Werlin, S.L., Troendle, D., Tang, G., Slivka, A., et al. (2019/04/01). Chronic Pancreatitis. Journal of Pediatric Gastroenterology and Nutrition *68*. 10.1097/MPG.0000000000002279.
14. LaRusch, J., and Whitcomb, D.C. (2011 Sep). Genetics of pancreatitis. Current opinion in gastroenterology *27*. 10.1097/MOG.0b013e328349e2f8.

759 15. Whitcomb, D.C., Gorry, M.C., Preston, R.A., Furey, W., Sossenheimer, M.J.,
760 Ulrich, C.D., Martin, S.P., Gates, L.K., Amann, S.T., Toskes, P.P., et al. (1996).
761 Hereditary pancreatitis is caused by a mutation in the cationic trypsinogen gene.
762 Nature Genetics *14*, 141-145. 10.1038/ng1096-141.
763 16. Howes, N., Lerch, M.M., Greenhalf, W., Stocken, D.D., Ellis, I., Simon, P.,
764 Truninger, K., Ammann, R., Cavallini, G., Charnley, R.M., et al. (2004). Clinical and
765 genetic characteristics of hereditary pancreatitis in Europe. Clinical
766 Gastroenterology and Hepatology *2*, 252-261. 10.1016/s1542-3565(04)00013-8.
767 17. Schnúr, A., Beer, S., Witt, H., Hegyi, P., and Sahin-Tóth, M. (2014). Functional
768 effects of 13 rare PRSS1 variants presumed to cause chronic pancreatitis. Gut *63*,
769 337. 10.1136/gutjnl-2012-304331.
770 18. Whitcomb, D.C. (2010). Genetic Aspects of Pancreatitis. Annual Review of
771 Medicine *61*, 413-424. 10.1146/annurev.med.041608.121416.
772 19. Threadgold, J., Greenhalf, W., Ellis, I., Howes, N., Lerch, M.M., Simon, P., Jansen,
773 J., Charnley, R., Laugier, R., Frulloni, L., et al. (2002). The N34S mutation of
774 SPINK1 (PSTI) is associated with a familial pattern of idiopathic chronic
775 pancreatitis but does not cause the disease. Gut *50*, 675. 10.1136/gut.50.5.675.
776 20. Grocock, C.J., Rebours, V., Delhaye, M.N., Andrén-Sandberg, A., Weiss, F.U.,
777 Mountford, R., Harcus, M.J., Niemczyck, E., Vitone, L.J., Dodd, S., et al. (2010).
778 The variable phenotype of the p.A16V mutation of cationic trypsinogen (PRSS1)
779 in pancreatitis families. Gut *59*, 357. 10.1136/gut.2009.186817.
780 21. Ooi, C.Y., Dorfman, R., Cipolli, M., Gonska, T., Castellani, C., Keenan, K.,
781 Freedman, S.D., Zielenski, J., Berthiaume, Y., Corey, M., et al. (2011). Type of
782 CFTR Mutation Determines Risk of Pancreatitis in Patients With Cystic Fibrosis.
783 Gastroenterology *140*, 153-161. 10.1053/j.gastro.2010.09.046.
784 22. Moniaux, N., Andrianifahanana, M., Brand, R.E., and Batra, S.K. (2004). Multiple
785 roles of mucins in pancreatic cancer, a lethal and challenging malignancy. British
786 Journal of Cancer *91*, 1633-1638. 10.1038/sj.bjc.6602163.
787 23. Viktoria Venglovecz, P.H., 2 Michael A. Gray3 (07/04/2021). Ion Channels in
788 Pancreatic Duct Epithelial Cells in Health and Disease. Pancreapedia: The
789 Exocrine Pancreas Knowledge Base. 10.3998/panc.2021.08.
790 24. Richter, L.D., Ruderfer, D.M., Peterson, J.F., and Bastarache, L.A. (2025). Beyond
791 Carrier Status: CFTR Heterozygosity as an Overlooked Clinical Risk Factor for
792 Pancreatitis. Clinical Genetics *n/a*. https://doi.org/10.1111/cge.14780.
793 25. Zoller, H., Egg, M., Graziadei, I., Creus, M., Janecke, A.R., Löffler-Ragg, J., and
794 Vogel, W. (2007). CFTR gene mutations in pancreatitis: Frequency and clinical
795 manifestations in an Austrian patient cohort. Wiener klinische Wochenschrift *119*,
796 527-533. 10.1007/s00508-007-0849-5.
797 26. Witt, H. (2003). Chronic pancreatitis and cystic fibrosis. Gut *52*, ii31.
798 10.1136/gut.52.suppl_2.ii31.
799 27. Truninger, K., Malik, N., Ammann, R.W., Muellhaupt, B., Seifert, B., Müller, H.J.,
800 and Blum, H.E. (2001). Mutations of the cystic fibrosis gene in patients with chronic
801 pancreatitis. The American journal of gastroenterology *96*, 2657-2661.
802 10.1111/j.1572-0241.2001.04047.x.
803 28. Kiesewetter, S., Macek, M., Davis, C., Curristin, S.M., Chu, C.S., Graham, C.,
804 Shrimpton, A.E., Cashman, S.M., Tsui, L.C., Mickle, J., et al. (1993). A mutation in

805 CFTR produces different phenotypes depending on chromosomal background.
806 Nature Genetics *5*, 274-278. 10.1038/ng1193-274.
807 29. Noone, P.G., Zhou, Z., Silverman, L.M., Jowell§, P.S., Knowles, M.R., and Cohn§,
808 J.A. (2001). Cystic fibrosis gene mutations and pancreatitis risk: Relation to
809 epithelial ion transport and trypsin inhibitor gene mutations. Gastroenterology *121*,
810 1310-1319. 10.1053/gast.2001.29673.
811 30. Audrézet, M.-P., Chen, J.-M., Maréchal, C.L., Ruszniewski, P., Robaszkiewicz, M.,
812 Raguénès, O., Quéré, I., Scotet, V., and Férec, C. (2002). Determination of the
813 relative contribution of three genes–the cystic fibrosis transmembrane
814 conductance regulator gene, the cationic trypsinogen gene, and the pancreatic
815 secretory trypsin inhibitor gene–to the etiology of idiopathic chronic pancreatitis.
816 European Journal of Human Genetics *10*, 100-106. 10.1038/sj.ejhg.5200786.
817 31. Lukacs, G.L., and Verkman, A.S. (2012). CFTR: folding, misfolding and correcting
818 the ΔF508 conformational defect. Trends in Molecular Medicine *18*, 81-91.
819 10.1016/j.molmed.2011.10.003.
820 32. Cohn, J.A., Friedman, K.J., Noone, P.G., Knowles, M.R., Silverman, L.M., and
821 Jowell, P.S. (1998-09-03). Relation between Mutations of the Cystic Fibrosis Gene
822 and Idiopathic Pancreatitis. New England Journal of Medicine *339*.
823 10.1056/NEJM199809033391002.
824 33. Wiseman, A.J., and Ooi, C.Y. (2021). Clinical Pancreatology for Practising
825 Gastroenterologists and Surgeons 10.1002/9781119570097.ch47.
826 34. Ooi, C.Y., Dupuis, A., Ellis, L., Jarvi, K., Martin, S., Ray, P.N., Steele, L., Kortan,
827 P., Gonska, T., Dorfman, R., et al. (2014). Does extensive genotyping and nasal
828 potential difference testing clarify the diagnosis of cystic fibrosis among patients
829 with single-organ manifestations of cystic fibrosis? Thorax *69*, 254.
830 10.1136/thoraxjnl-2013-203832.
831 35. Clancy, J.P., Rowe, S.M., Accurso, F.J., Aitken, M.L., Amin, R.S., Ashlock, M.A.,
832 Ballmann, M., Boyle, M.P., Bronsveld, I., Campbell, P.W., et al. (2012). Results of
833 a phase IIa study of VX-809, an investigational CFTR corrector compound, in
834 subjects with cystic fibrosis homozygous for the F508del-CFTR mutation. Thorax
835 *67*, 12-18. 10.1136/thoraxjnl-2011-200393.
836 36. Flume, P.A., Liou, T.G., Borowitz, D.S., Li, H., Yen, K., Ordoñez, C.L., and Geller,
837 D.E. (2012). Ivacaftor in subjects with cystic fibrosis who are homozygous for the
838 F508del-CFTR mutation. Chest *142*, 718-724. 10.1378/chest.11-2672.
839 37. Ishiguro, H., Yamamoto, A., Nakakuki, M., Yi, L., Ishiguro, M., Yamaguchi, M.,
840 Kondo, S., and Mochimaru, Y. (2012). Physiology and pathophysiology of
841 bicarbonate secretion by pancreatic duct epithelium. Nagoya J Med Sci *74*, 1-18.
842 38. Ramsey, B.W., Davies, J., McElvaney, N.G., Tullis, E., Bell, S.C., Dřevínek, P.,
843 Griese, M., McKone, E.F., Wainwright, C.E., Konstan, M.W., et al. (2011). A CFTR
844 potentiator in patients with cystic fibrosis and the G551D mutation. N Engl J Med
845 *365*, 1663-1672. 10.1056/NEJMoa1105185.
846 39. van Mourik, P., Michel, S., Vonk, A.M., Beekman, J.M., van der Ent, C.K., van
847 Mourik, P., Michel, S., Vonk, A.M., Beekman, J.M., and van der Ent, C.K. (2020-
848 06-03). Rationale and design of the HIT-CF organoid study: stratifying cystic
849 fibrosis patients based on intestinal organoid response to different CFTR-

850 modulators. Translational Medicine Communications 2020 5:1 *5*. 10.1186/s41231-
851 020-00060-3.
852 40. Dekkers, J.F., Wiegerinck, C.L., de Jonge, H.R., Bronsveld, I., Janssens, H.M., de
853 Winter-de Groot, K.M., Brandsma, A.M., de Jong, N.W.M., Bijvelds, M.J.C.,
854 Scholte, B.J., et al. (2013-06-02). A functional CFTR assay using primary cystic
855 fibrosis intestinal organoids. Nature Medicine 2013 19:7 *19*. 10.1038/nm.3201.
856 41. McCarron, A., Parsons, D., and Donnelley, M. (2021). Animal and Cell Culture
857 Models for Cystic Fibrosis: Which Model Is Right for Your Application? The
858 American Journal of Pathology *191*, 228-242. 10.1016/j.ajpath.2020.10.017.
859 42. Boj, Sylvia F., Hwang, C.-I., Baker, Lindsey A., Chio, Iok In C., Engle,
860 Dannielle D., Corbo, V., Jager, M., Ponz-Sarvise, M., Tiriac, H., Spector, Mona S.,
861 et al. (2015). Organoid Models of Human and Mouse Ductal Pancreatic Cancer.
862 Cell *160*, 324-338. 10.1016/j.cell.2014.12.021.
863 43. Tiriac, H., Belleau, P., Engle, D.D., Plenker, D., Deschênes, A., Somerville, T.,
864 Froeling, F.E.M., Burkhart, R.A., Denroche, R.E., Jang, G.-H., et al. (2018).
865 Organoid profiling identifies common responders to chemotherapy in pancreatic
866 cancer. Cancer Discovery *8*, CD-18-0349. 10.1158/2159-8290.cd-18-0349.
867 44. Kim, J., Hoffman, J.P., Alpaugh, R.K., Rhim, A.D., Rhimm, A.D., Reichert, M.,
868 Stanger, B.Z., Furth, E.E., Sepulveda, A.R., Yuan, C.-X., et al. (2013). An iPSC
869 Line from Human Pancreatic Ductal Adenocarcinoma Undergoes Early to Invasive
870 Stages of Pancreatic Cancer Progression. Cell Reports *3*, 2088-2099.
871 10.1016/j.celrep.2013.05.036.
872 45. Grossman, J.E., Muthuswamy, L., Huang, L., Akshinthala, D., Perea, S., Gonzalez,
873 R.S., Tsai, L.L., Cohen, J., Bockorny, B., Bullock, A.J., et al. (2021). Organoid
874 Sensitivity Correlates with Therapeutic Response in Patients with Pancreatic
875 Cancer. Clinical Cancer Research *28*, clincanres.4116.2020. 10.1158/1078-
876 0432.ccr-20-4116.
877 46. Gulay, K.C.M., Zhang, X., Pantazopoulou, V., Patel, J., Esparza, E., Babu, D.S.P.,
878 Ogawa, S., Weitz, J., Ng, I., Mose, E.S., et al. (2023). Dual inhibition of KRASG12D
879 and pan-ERBB is synergistic in pancreatic ductal adenocarcinoma. Cancer
880 Research. 10.1158/0008-5472.can-23-1313.
881 47. Ponz-Sarvise, M., Corbo, V., Tiriac, H., Engle, D.D., Frese, K.K., Oni, T.E., Hwang,
882 C.-I., Öhlund, D., Chio, I.I.C., Baker, L.A., et al. (2019). Identification of Resistance
883 Pathways Specific to Malignancy Using Organoid Models of Pancreatic Cancer.
884 Clinical Cancer Research *25*, 6742-6755. 10.1158/1078-0432.ccr-19-1398.
885 48. Hou, S., Tiriac, H., Sridharan, B.P., Scampavia, L., Madoux, F., Seldin, J., Souza,
886 G.R., Watson, D., Tuveson, D., and Spicer, T.P. (2018). Advanced Development
887 of Primary Pancreatic Organoid Tumor Models for High-Throughput Phenotypic
888 Drug Screening. SLAS Discovery *23*, 574-584. 10.1177/2472555218766842.
889 49. Wolff, R.A., Wang-Gillam, A., Alvarez, H., Tiriac, H., Engle, D., Hou, S., Groff, A.F.,
890 Lucas, A.S., Bernard, V., Allenson, K., et al. (2018). Dynamic changes during the
891 treatment of pancreatic cancer. Oncotarget *9*, 14764-14790.
892 10.18632/oncotarget.24483.
893 50. Lumibao, J.C., Okhovat, S.R., Peck, K.L., Lin, X., Lande, K., Yomtoubian, S., Ng,
894 I., Tiriac, H., Lowy, A.M., Zou, J., and Engle, D.D. (2023). The impact of

895 extracellular matrix on the precision medicine utility of pancreatic cancer patient-
896 derived organoids. JCI Insight *9*, e172419. 10.1172/jci.insight.172419.
897 51. Letai, A., Bhola, P., and Welm, A.L. (2022). Functional precision oncology: Testing
898 tumors with drugs to identify vulnerabilities and novel combinations. Cancer Cell
899 *40*, 26-35. 10.1016/j.ccell.2021.12.004.
900 52. Boilève, A., Cartry, J., Goudarzi, N., Bedja, S., Mathieu, J.R.R., Bani, M.-A.,
901 Nicolle, R., Mouawia, A., Bouyakoub, R., Nicotra, C., et al. (2024). Organoids for
902 functional precision medicine in advanced pancreatic cancer. Gastroenterology.
903 10.1053/j.gastro.2024.05.032.
904 53. Shik Mun, K., Arora, K., Huang, Y., Yang, F., Yarlagadda, S., Ramananda, Y.,
905 Abu-El-Haija, M., Palermo, J.J., Appakalai, B.N., Nathan, J.D., et al. (2019-07-16).
906 Patient-derived pancreas-on-a-chip to model cystic fibrosis-related disorders.
907 Nature Communications 2019 10:1 *10*. 10.1038/s41467-019-11178-w.
908 54. Bankhead, P., Loughrey, M.B., Fernández, J.A., Dombrowski, Y., McArt, D.G.,
909 Dunne, P.D., McQuaid, S., Gray, R.T., Murray, L.J., Coleman, H.G., et al. (2017).
910 QuPath: Open source software for digital pathology image analysis. Scientific
911 Reports *7*, 16878. 10.1038/s41598-017-17204-5.
912 55. Esposito, I., Hruban, R.H., Verbeke, C., Terris, B., Zamboni, G., Scarpa, A.,
913 Morohoshi, T., Suda, K., Luchini, C., Klimstra, D.S., et al. (2020/06/01). Guidelines
914 on the histopathology of chronic pancreatitis. Recommendations from the working
915 group for the international consensus guidelines for chronic pancreatitis in
916 collaboration with the International Association of Pancreatology, the American
917 Pancreatic Association, the Japan Pancreas Society, and the European
918 Pancreatic Club. Pancreatology *20*. 10.1016/j.pan.2020.04.009.
919 56. Stirling, D.R., Swain-Bowden, M.J., Lucas, A.M., Carpenter, A.E., Cimini, B.A.,
920 Goodman, A., Stirling, D.R., Swain-Bowden, M.J., Lucas, A.M., Carpenter, A.E.,
921 et al. (2021-09-10). CellProfiler 4: improvements in speed, utility and usability.
922 BMC Bioinformatics 2021 22:1 *22*. 10.1186/s12859-021-04344-9.
923 57. SW, W., and S, A. (08/24/2018). FastQ Screen: A tool for multi-genome mapping
924 and quality control - PubMed. F1000Research *7*.
925 10.12688/f1000research.15931.2.
926 58. Martin, M. (2011/05/02). Cutadapt removes adapter sequences from high-
927 throughput sequencing reads. EMBnet.journal *17*. 10.14806/ej.17.1.200.
928 59. JM, M., S, C.-S., M, D., JG, M., T, H., I, J., JE, L., C, A., I, B., R, B., et al.
929 (01/06/2025). GENCODE 2025: reference gene annotation for human and mouse
930 - PubMed. Nucleic acids research *53*. 10.1093/nar/gkae1078.
931 60. VA, S., T, G.-L., K, H., N, B., HC, C., PA, K., TD, M., KD, P., F, T.-N., D, A., et al.
932 (2017 May). Evaluation of GRCh38 and de novo haploid genome assemblies
933 demonstrates the enduring quality of the reference assembly - PubMed. Genome
934 research *27*. 10.1101/gr.213611.116.
935 61. Dobin, A., Davis, C.A., Schlesinger, F., Drenkow, J., Zaleski, C., Jha, S., Batut, P.,
936 Chaisson, M., and Gingeras, T.R. (2013). STAR: ultrafast universal RNA-seq
937 aligner. Bioinformatics *29*, 15-21. 10.1093/bioinformatics/bts635.
938 62. Love, M.I., Huber, W., and Anders, S. (2014). Moderated estimation of fold change
939 and dispersion for RNA-seq data with DESeq2. Genome Biology *15*, 550.
940 10.1186/s13059-014-0550-8.

63. Gaujoux, R., Seoighe, C., Gaujoux, R., and Seoighe, C. (2010-07-02). A flexible R package for nonnegative matrix factorization. BMC Bioinformatics 2010 11:1 *11*. 10.1186/1471-2105-11-367.
64. Kim, H., and Park, H. (2007/06/15). Sparse non-negative matrix factorizations via alternating non-negativity-constrained least squares for microarray data analysis. Bioinformatics *23*. 10.1093/bioinformatics/btm134.
65. Mootha, V.K., Lindgren, C.M., Eriksson, K.-F., Subramanian, A., Sihag, S., Lehar, J., Puigserver, P., Carlsson, E., Ridderstråle, M., Laurila, E., et al. (2003). PGC-1α-responsive genes involved in oxidative phosphorylation are coordinately downregulated in human diabetes. Nature Genetics *34*, 267-273. 10.1038/ng1180.
66. A, S., P, T., VK, M., S, M., BL, E., MA, G., A, P., SL, P., TR, G., ES, L., and JP, M. (10/25/2005). Gene set enrichment analysis: a knowledge-based approach for interpreting genome-wide expression profiles - PubMed. Proceedings of the National Academy of Sciences of the United States of America *102*. 10.1073/pnas.0506580102.
67. Xu, Y., Nipper, M.H., Dominguez, A.A., Ye, Z., Akanuma, N., Lopez, K., Deng, J.J., Arenas, D., Sanchez, A., Sharkey, F.E., et al. (2024-01-27). Reconstitution of human PDAC using primary cells reveals oncogenic transcriptomic features at tumor onset. Nature Communications 2024 15:1 *15*. 10.1038/s41467-024-45097-2.
68. DA, B., P, T., JS, B., SY, K., SE, M., IF, D., AC, S., P, S., E, M., C, S., et al. (11/05/2009). Systematic RNA interference reveals that oncogenic KRAS-driven cancers require TBK1 - PubMed. Nature *462*. 10.1038/nature08460.
69. Tosti, L., Hang, Y., Debnath, O., Tiesmeyer, S., Trefzer, T., Steiger, K., Ten, F.W., Lukassen, S., Ballke, S., Kühl, A.A., et al. (2021). Single-Nucleus and In Situ RNA–Sequencing Reveal Cell Topographies in the Human Pancreas. Gastroenterology *160*, 1330-1344.e1311. 10.1053/j.gastro.2020.11.010.
70. Mastromatteo, S., Chen, A., Gong, J., Lin, F., Thiruvahindrapuram, B., Sung, W.W., Whitney, J., Wang, Z., Patel, R.V., Keenan, K., et al. (2022 Oct 20). High-quality read-based phasing of cystic fibrosis cohort informs genetic understanding of disease modification. Human Genetics and Genomics Advances *4*. 10.1016/j.xhgg.2022.100156.
71. Lou, H., Xie, B., Wang, Y., Gao, Y., and Xu, S. (2023-01-01). Improved NGS variant calling tool for the PRSS1–PRSS2 locus. Gut *72*. 10.1136/gutjnl-2022-327203.
72. Surendran, R.P., Visser, M.E., Heemelaar, S., Wang, J., Peter, J., Defesche, J.C., Kuivenhoven, J.A., Hosseini, M., Péterfy, M., Kastelein, J.J.P., et al. (2012/08/01). Journal of Internal Medicine | Wiley Online Library. Journal of Internal Medicine *272*. 10.1111/j.1365-2796.2012.02516.x.
73. Hang, S.M., Hegele, R.A., and Berberich, A.J. (2023 Feb 1). Genetic determinants of pancreatitis: relevance in severe hypertriglyceridemia. Current Opinion in Lipidology *34*. 10.1097/MOL.0000000000000866.
74. Cuppens, H., Lin, W., Jaspers, M., Costes, B., Teng, H., Vankeerberghen, A., Jorissen, M., Droogmans, G., Reynaert, I., Goossens, M., et al. (1998/01/15). Polyvariant mutant cystic fibrosis transmembrane conductance regulator genes. The polymorphic (Tg)m locus explains the partial penetrance of the T5

987 polymorphism as a disease mutation. The Journal of Clinical Investigation *101*.
988 10.1172/JCI639.
989 75. JH, L., JH, C., W, N., JW, H., J, C., SY, S., SW, P., DS, K., JH, Y., Y, S., et al.
990 (09/15/2003). A haplotype-based molecular analysis of CFTR mutations
991 associated with respiratory and pancreatic diseases - PubMed. Human molecular
992 genetics *12*. 10.1093/hmg/ddg243.
993 76. A, S., J, L., X, S., A, A., J, L., R, H., P, C., RE, B., MA, A., ME, M., et al. (2011
994 Jan). Combined bicarbonate conductance-impairing variants in CFTR and SPINK1
995 variants are associated with chronic pancreatitis in patients without cystic fibrosis
996 - PubMed. Gastroenterology *140*. 10.1053/j.gastro.2010.10.045.
997 77. J, L., J, J., IJ, G., MD, L., HW, P., RE, B., A, G., MA, A., PA, B., D, C., et al.
998 (07/17/2014). Mechanisms of CFTR functional variants that impair regulated
999 bicarbonate permeation and increase risk for pancreatitis but not for cystic fibrosis
1000 - PubMed. PLoS genetics *10*. 10.1371/journal.pgen.1004376.
1001 78. Haggie, P.M., Phuan, P.-W., Tan, J.-A., Xu, H., Avramescu, R.G., Perdomo, D.,
1002 Zlock, L., Nielson, D.W., Finkbeiner, W.E., Lukacs, G.L., and Verkman, A.S. (2016
1003 Nov 28). Correctors and Potentiators Rescue Function of the Truncated W1282X-
1004 Cystic Fibrosis Transmembrane Regulator (CFTR) Translation Product. The
1005 Journal of Biological Chemistry *292*. 10.1074/jbc.M116.764720.
1006 79. van Willigen, M., Vonk, A.M., Yeoh, H.Y., Kruisselbrink, E., Kleizen, B., van der
1007 Ent, C.K., Egmond, M.R., de Jonge, H.R., Braakman, I.A.-O., Beekman, J.M., and
1008 van der Sluijs, P.A.-O. (2019). Folding-function relationship of the most common
1009 cystic fibrosis-causing CFTR conductance mutants. LID - 10.26508/lsa.201800172
1010 [doi] LID - e201800172.
1011 80. Modiano, G., Bombieri, C., Ciminelli, B.M., Belpinati, F., Giorgi, S., Georges, M.d.,
1012 Scotet, V., Pompei, F., Ciccacci, C., Guittard, C., et al. (2004-11-10). A large-scale
1013 study of the random variability of a coding sequence: a study on the CFTR gene.
1014 European Journal of Human Genetics 2005 13:2 *13*. 10.1038/sj.ejhg.5201306.
1015 81. BM, C., A, B., C, B., F, P., M, G., C, C., A, B., A, H., P, Z., T, P., et al. (2007 Jan).
1016 Highly preferential association of NonF508del CF mutations with the M470 allele -
1017 PubMed. Journal of cystic fibrosis : official journal of the European Cystic Fibrosis
1018 Society *6*. 10.1016/j.jcf.2006.04.003.
1019 82. Zielenski, J., Patrizio, P., Corey, M., Handelin, B., Markiewicz, D., Asch, R., and
1020 Tsui, L.C. (1995). CFTR gene variant for patients with congenital absence of vas
1021 deferens. Am J Hum Genet *57*, 958-960.
1022 83. D, Z., R, B., and L, W. (2020 Jan). The Cystic Fibrosis Transmembrane
1023 Conductance Regulator 470 Met Allele Is Associated with an Increased Risk of
1024 Chronic Pancreatitis in Both Asian and Caucasian Populations: A Meta-Analysis -
1025 PubMed. Genetic testing and molecular biomarkers *24*. 10.1089/gtmb.2019.0199.
1026 84. Iso, M., Suzuki, M., Yanagi, K., Minowa, K., Sakurai, Y., Nakano, S., Satou, K.,
1027 Shimizu, T., Kaname, T., Iso, M., et al. (2019-04-11). The CFTR gene variants in
1028 Japanese children with idiopathic pancreatitis. Human Genome Variation 2019 6:1
1029 *6*. 10.1038/s41439-019-0049-7.
1030 85. Angyal, D., Kleinfelder, K., Ciciriello, F., Groeneweg, T.A., Marchi, G.D., Pretis,
1031 N.d., Bernardoni, L., Rodella, L., Tomba, F., Angelis, P.D., et al. (2024). CFTR

function is impaired in a subset of patients with pancreatitis carrying rare CFTR variants. Pancreatology *24*, 394-403. 10.1016/j.pan.2024.03.005.

86. El-Seedy, A., Girodon, E., Norez, C., Pajaud, J., Pasquet, M.-C., Becdelièvre, A.d., Bienvenu, T., Georges, M.d., Cabet, F., Lalau, G., et al. (2012/11/01). CFTR mutation combinations producing frequent complex alleles with different clinical and functional outcomes. Human Mutation *33*. 10.1002/humu.22129.

87. Doss, C.G.P., Rajasekaran, R., Sudandiradoss, C., Ramanathan, K., Purohit, R., and Sethumadhavan, R. (2008 May 14). A novel computational and structural analysis of nsSNPs in CFTR gene. Genomic Medicine *2*. 10.1007/s11568-008-9019-8.

88. Meléndez-Montañez, J.M., Jesús-Rojas, W.D., Meléndez-Montañez, J.M., and De Jesús-Rojas, W. (2023-01-31). CFTR-Related Metabolic Syndrome: Genetic Variants Increasing Pancreatitis Risk in the Pediatric Puerto Rican Population. Children 2023, Vol. 10, Page 280 *10*. 10.3390/children10020280.

89. S, R., I, V., A, M., S, B., J, R., RM, C., and SM, R. (2016 Sep-Oct). Chronic pancreatitis: Do serum biomarkers provide an association with an inflammageing phenotype? - PubMed. Pancreatology : official journal of the International Association of Pancreatology (IAP) ... [et al.] *16*. 10.1016/j.pan.2016.08.004.

90. Engle, D.D., Tiriac, H., Rivera, K.D., Pommier, A., Whalen, S., Oni, T.E., Alagesan, B., Lee, E.J., Yao, M.A., Lucito, M.S., et al. (2019). The glycan CA19-9 promotes pancreatitis and pancreatic cancer in mice. Science *364*, 1156-1162. 10.1126/science.aaw3145.

91. CM, A., BM, G., KK, T., C, L.-M., N, T., PK, M., KE, D., ES, C., CJ, H., JC, H., et al. (09/11/2012). EGF receptor is required for KRAS-induced pancreatic tumorigenesis - PubMed. Cancer cell *22*. 10.1016/j.ccr.2012.07.024.

92. Cheng, S.H., Gregory, R.J., Marshall, J., Paul, S., Souza, D.W., White, G.A., O'Riordan, C.R., and Smith, A.E. (1990/11/16). Defective intracellular transport and processing of CFTR is the molecular basis of most cystic fibrosis. Cell *63*. 10.1016/0092-8674(90)90148-8.

93. Wilson, J.S., Pirola, R.C., and Apte, M.V. (2018). Epidemiology and Etiology of Alcohol-Induced Pancreatitis. The Pancreas. 10.1002/9781119188421.ch13.

94. Maléth, J., Balázs, A., Pallagi, P., Balla, Z., Kui, B., Katona, M., Judák, L., Németh, I., Kemény, L.V., Rakonczay, Z., et al. (2015). Alcohol Disrupts Levels and Function of the Cystic Fibrosis Transmembrane Conductance Regulator to Promote Development of Pancreatitis. Gastroenterology *148*, 427-439.e416. 10.1053/j.gastro.2014.11.002.

95. MY, P., and ZM, S. (2022 Jun). Current clinical opinion on CFTR dysfunction and patient risk of pancreatitis: diagnostic and therapeutic considerations - PubMed. Expert review of gastroenterology & hepatology *16*. 10.1080/17474124.2022.2084072.

96. Gullo, L., Pezzilli, R., Bellanova, B., D'Ambrosi, A., Alvisi, V., and Barbara, L. (1991). Influence of the thyroid on exocrine pancreatic function. Gastroenterology *100*, 1392-1396.

97. Komar, H.M., Hart, P.A., Cruz-Monserrate, Z., Conwell, D.L., and Lesinski, G.B. (2017). Local and Systemic Expression of Immunomodulatory Factors in Chronic Pancreatitis. Pancreas *46*, 986-993. 10.1097/mpa.0000000000000896.

98. Yasuda, M., Ito, T., Oono, T., Kawabe, K., Kaku, T., Igarashi, H., Nakamura, T., and Takayanagi, R. (2008 Nov 14). Fractalkine and TGF-β1 levels reflect the severity of chronic pancreatitis in humans. World Journal of Gastroenterology : WJG *14*. 10.3748/wjg.14.6488.
99. Bedwell, D.M., Kaenjak, A., Benos, D.J., Bebok, Z., Bubien, J.K., Hong, J., Tousson, A., Clancy, J.P., Sorscher, E.J., Bedwell, D.M., et al. (1997/11). Suppression of a CFTR premature stop mutation in a bronchial epithelial cell line. Nature Medicine 1997 3:11 *3*. 10.1038/nm1197-1280.
100. Mourik, P.V., Haaren, P.v., Kruisselbrink, E., Korkmaz, C., Janssens, H.M., Groot, K.M.d.W.d., Ent, C.K.v.d., Hagemeijer, M.C., and Beekman, J.M. (2020). R117H-CFTR function and response to VX-770 correlate with mRNA and protein expression in intestinal organoids. Journal of Cystic Fibrosis *19*, 728-732. 10.1016/j.jcf.2020.02.001.
101. J, R., C, P.-S., IAI, S., C, M., S, A., R, F., and G, O. (05/21/2022). New drugs in cystic fibrosis: what has changed in the last decade? - PubMed. Therapeutic advances in chronic disease *13*. 10.1177/20406223221098136.
102. DM, C., NL, Q., ML, F., CR, E., J, D., NV, D., SH, R., RC, B., and M, G. (07/23/2014). Potentiator ivacaftor abrogates pharmacological correction of ΔF508 CFTR in cystic fibrosis - PubMed. Science translational medicine *6*. 10.1126/scitranslmed.3008680.
103. Carpenter, E.S., Elhossiny, A.M., Kadiyala, P., Li, J., McGue, J., Griffith, B.D., Zhang, Y., Edwards, J., Nelson, S., Lima, F., et al. (2023/06/01). Analysis of Donor Pancreata Defines the Transcriptomic Signature and Microenvironment of Early Neoplastic Lesions. Cancer Discovery *13*. 10.1158/2159-8290.CD-23-0013.
104. Mello, S.S., Flowers, B.M., Mazur, P.K., Lee, J.J., Müller, F., Denny, S.K., Ferreira, S., Hanson, K., Kim, S.K., Greenleaf, W.J., et al. (2023-2-27). Multifaceted role for p53 in pancreatic cancer suppression. Proceedings of the National Academy of Sciences *120*. 10.1073/pnas.2211937120.

1108 **Tables**

1109

1110 **Table 1.** Characteristics of patients (n=51).

Demographics	***PDO established (n=36)***	***PDO not established (n=12)/ in progress (n=3)***
Age, y, average (SD)	37(18%)	41 (17%)/ 37(21%)
Female sex, n (%)	24 (66%)	7 (58%)/ 2 (66%)
Male sex, n (%)	12 (33%)	5 (42%)/ 1 (33%)
Race		
White, n (%)	28 (77%)	7 (58%) / 1 (33%)
Hispanic, n (%)	4 (11%)	1 (8.3%) / 2 (66%)
Black, n (%)	1 (2.7%)	1 (8.3%)
Multi-racial, n (%)	1 (2.7%)	2 (16.6%)
Not reported	2 (5.5%)	0 (0%)
Procedure		
Partial Pancreatectomy (total =16), n (%)	9 (25%)	7 (58%)/ 0 (0%)
TPIAT (total = 35), n (%)	27 (75%)	5 (42%)/ 3 (100%)
Etiology		
Genetic	16 (44%)	2 (16.6%)/ 0(0%)
Idiopathic	12 (33%)	8 (66%)/ 1(33%)
Alcohol	3 (8.3%)	0(0%)/ 0(0%)
Obstruction	1 (2.7%)	0(0%)/ 0(0%)
Solid-pseudopapillary neoplasm	1 (2.7%)	0(0%)/ 0(0%)
Divisium + Genetic	2 (5.5%)	2 (16.6%) / 1(33%)
Groove	1 (2.7%)	0(0%)/ 0(0%)
Sphincter of Oddi dysfunction	0 (0%)	0(0%)/1(33%)
Mutations		
PRSS1	7 (19%)	2 (16%)/ 0(0%)
SPINK1	6 (17%)	0 (0%)/ 0(0%)
CFTR	10 (28%)	2 (17%)/ 0(0%)

1111

1112 **Table S1. Patient sample information and downstream sequencing technologies applied to patient derived organoids (PDOs).**

Sample	Patient	Sex	Age	Race	Type	Etiology	Procedure	PDO	Targeted sequencing	WES-PDO	WGS-PDO	WGS-PT	RNA seq
hCP01	1	F	ADT	W,NH	CP	I	PP	Y	Y	N	N	Y	Y
hCP02	2	F	ADT	W,NH	SPN	SPN	PP	Y	N	N	N	N	N
hCP03	3	F	ADT	W,NH	CP	I	PP	Y	Y	N	N	Y	Y
hCP04	3	F	ADT	W,NH	CP	I	PP	N	NA	NA	NA	N	NA
hCP05	4	F	ADT	W,NH	CP	I	PP	N	NA	NA	NA	N	NA
hCP06	5	F	ADT	W	RAP	G, D	TPIAT	N	NA	NA	NA	N	NA
hCP07	6	F	ADT	W,NH	CP	I	PP*	Y	N	N	Y	Y	Y
hCP08	7	F	PED	W,NH	RAP to CP	G	TPIAT	Y	Y	Y	N	Y	Y
hCP09	8	F	ADT	W,NH	CP	I	PP	Y	N	N	N	N	N
hCP10	9	M	ADT	W,NH	CP	I	PP	N	NA	NA	NA	N	NA
hCP11	10	F	ADT	W,NH	RAP to CP	G	TPIAT	Y	Y	Y	N	Y	Y
hCP12	11	F	PED	W,NH	RAP to CP	G	TPIAT	Y	N	N	N	N	N
hCP13	12	F	ADT	W,NH	RAP to CP	G	TPIAT	Y	N	N	N	N	N
hCP14	13	M	PED	W,NH	RAP to CP	G	TPIAT	N	NA	NA	NA	N	NA
hCP15	14	M	ADT	W,NH	RAP to CP	A	TPIAT	Y	Y	Y	N	Y	Y
hCP16	15	F	ADT	W,NH	RAP to CP	O	TPIAT	Y	Y	N	Y	Y	Y
hCP17	16	F	PED	W,NH	RAP to CP	G	TPIAT	Y	Y	Y	N	Y	Y
hCP18	17	F	ADT	W,NH	CP	I	TPIAT	Y	N	N	Y	Y	Y
hCP19	18	F	ADT	Multi	CP	I	PP	N	NA	NA	NA	N	NA
hCP20	19	F	PED	W,NH	RAP to CP	I	TPIAT	Y	Y	Y	N	Y	Y

hCP21	20	M	ADT	W,NH	RAP to early CP	D	TPIAT	Y	N	N	N	N	N
hCP22	21	F	ADT	W,NH	CP	I	PP	Y	N	N	N	N	N
hCP23	22	F	PED	W,NH	RAP to CP	G	TPIAT	Y	N	N	N	N	N
hCP24	23	F	PED	W,NH	RAP	G	TPIAT	Y	N	N	Y	Y	Y
hCP25	24	F	PED	H	RAP to CP	I	TPIAT	Y	N	N	Y	Y	Y
hCP26	25	M	ADT	W,NH	CP	I	PP	Y	Y	N	N	Y	Y
hCP27	25	M	ADT	W,NH	CP	I	PP*	Y	N	N	Y	Y	Y
hCP28	26	F	ADT	H	RAP to CP	G	TPIAT	Y	N	N	Y	Y	Y
hCP29	27	M	ADT	W,NH	RAP to CP	A	TPIAT	Y	N	N	Y	Y	Y
hCP30	28	M	ADT	W,NH	RAP to early CP	G	TPIAT	Y	N	N	Y	Y	Y
hCP31	29	M	ADT	Multi	CP	I	PP	N	NA	NA	NA	N	NA
hCP32	30	M	ADT	W,NH	RAP to CP	G	TPIAT	Y	N	N	Y	Y	Y
hCP33	31	F	ADT	W	RAP to CP	I	PP	N	NA	NA	NA	N	NA
hCP34	32	M	ADT	W,NH	RAP to CP	I	TPIAT	N	NA	NA	NA	N	NA
hCP35	33	M	ADT	H	RAP to CP	G	TPIAT	Y	Y	N	N	Y	Y
hCP36	34	F	ADT	W,NH	RAP to CP	G	TPIAT	Y	N	N	Y	Y	Y
hCP37	35	F	PED	H	RAP to CP	G	TPIAT	N	NA	NA	NA	N	NA
hCP38	36	F	ADT	B	RAP to CP	Groove	TPIAT	Y	N	N	N	N	N
hCP39	37	M	ADT	B	CP	I	PP	N	NA	NA	NA	N	NA
hCP40	38	F	ADT	W,NH	RAP to CP	G	TPIAT	Y	N	N	N	N	N

hCP41	39	F	ADT	W,NH	RAP to CP	I	TPIAT	Y	N	N	N	N	N
hCP42	40	M	ADT	W,NH	RAP to CP	G	TPIAT	Y	N	N	N	N	N
hCP43	41	F	ADT	W,NH	RAP to CP	A	TPIAT	Y	N	N	N	N	N
hCP44	42	M	ADT	W,NH	RAP to early CP	G	TPIAT	Y	Y	N	N	Y	Y
hCP45	43	F	ADT	W,NH	RAP to CP	D	TPIAT	N	NA	NA	NA	N	NA
hCP46	44	M	ADT	H	RAP to early CP	I	TPIAT	IP	NA	NA	NA	N	NA
hCP47	45	F	ADT	W,NH	CP	SOD	TPIAT	IP	NA	NA	NA	N	NA
hCP48	46	F	ADT	Multi	CP	I	PP	Y	N	N	Y	Y	Y
hCP49	47	M	ADT	W,NH	RAP to CP	D, VATER	TPIAT	Y	N	N	Y	Y	Y
hCP50	48	F	ADT	H	RAP to early CP	D	TPIAT	IP	NA	NA	NA	N	NA
hCP51	49	F	ADT	H	RAP to early CP	D	TPIAT	Y	N	N	Y	Y	Y
hNAT02	50	M	ADT	W,NH	normal	Distal to NET		Y	N	N	N	N	Y
hNAT04	51	M	ADT	W,NH	normal	Adj to PDAC		Y	N	N	N	N	Y
hNAT07	53	M	ADT	W,NH	normal	Adj to ampullary tumor		Y	N	N	N	N	Y
hNAT09	54	M	ADT	W,NH	normal	Adj to PDAC		Y	N	N	N	N	Y
hNP03 Body	55	F	ADT	W,NH	normal	COD: anoxia	Organ donation	Y	N	N	N	N	Y
hNP03 Head	55	F	ADT	W,NH	normal	COD: anoxia	Organ donation	Y	N	N	Y	N	Y
hNP03 Tail	55	F	ADT	W,NH	normal	COD: anoxia	Organ donation	Y	N	N	Y	N	Y

hNP05 Body	56	M	ADT	H	normal	COD: cerebrovascular stroke	Organ donation	Y	N	N	N	N	Y
hNP05 Head	56	M	ADT	H	normal	COD: cerebrovascular stroke	Organ donation	Y	N	N	Y	N	Y
hNP05 Tail	56	M	ADT	H	normal	COD: cerebrovascular stroke	Organ donation	Y	N	N	Y	N	Y
hNP16 Body	57	M	ADT	W,NH	normal	COD: cerebrovascular stroke	Organ donation	Y	Y	N	N	N	Y
hNP16 Head	57	M	ADT	W,NH	normal	COD: cerebrovascular stroke	Organ donation	N	N	N	Y	N	Y
hNP16 Tail	57	M	ADT	W,NH	normal	COD: cerebrovascular stroke	Organ donation	Y	N	N	Y	N	Y

Abbreviations: Race: W-White, NH- non-Hispanic, H- Hispanic, B- Black, Multi- multi-racial; Sex: M-Male, F-Female; Age: ADT- Adult, PED- Pediatric Type: CP- chronic pancreatitis, SPN- Solid-pseudopapillary neoplasm, RAP- recurrent acute pancreatitis; Etiology: I- idiopathic, SPN- Solid-pseudopapillary neoplasm, G- genetic, D- divisum, A- alcohol, O- obstruction, SOD- Sphincter of Oddi Dysfunction, VATER- ampulla of Vater, NET- neuroendocrine tumor, PDAC- pancreatic ductal adenocarcinoma, Adj- adjacent, COD- cause of death; Procedure: PP- partial pancreatectomy, TPIAT- total pancreatectomy with islet auto transplantation; IP- in progress, Y- Yes, N- No, NA- not applicable, *- from pancreatic juice.

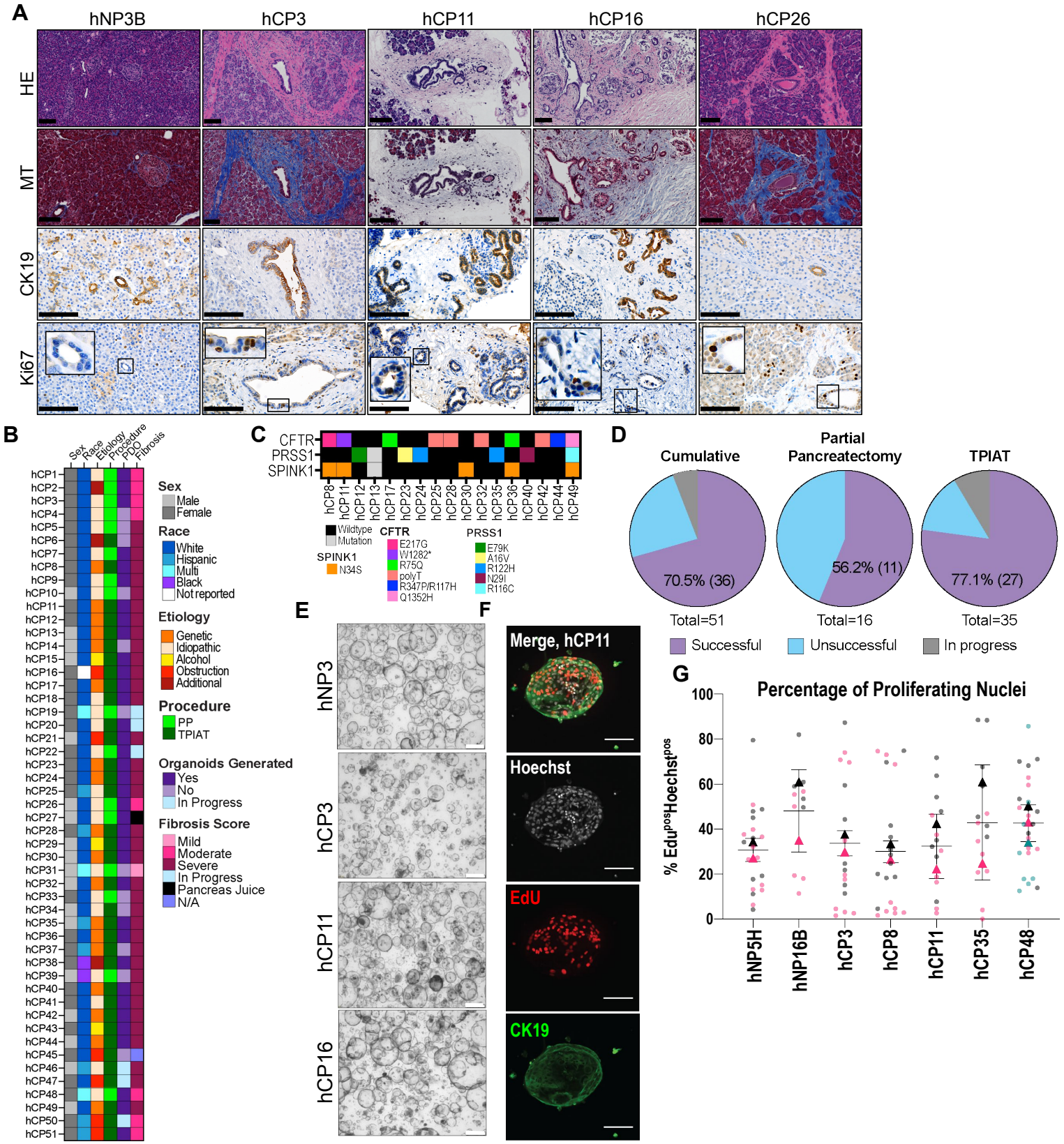

Figure 1. Generation of organoids from patients with human chronic pancreatitis (CP) with high effciency.

(A) Representative human normal pancreas (hNP) section displays characteristic ductal, acinar, and islet cells. Masson's trichrome (MT) staining highlights low degree of fibrosis in NP sample and varying severity in human CP (hCP) samples in blue. NP sample has high levels of cytokeratin 19 staining (CK19) in ductal epithelial cells, while CP samples have an altered ductal cell compartment. Ki-67 expression is low in NP sample and is altered or completely lost in hCP samples. Scale bar 100 µm. For diagram outlining generation procedure and histological features of samples that did not produce organoids see Figure S1.

(B) Patient sample cohort demographic, etiology, procedure for acquisition (total pancreatectomy with auto islet transplantation (TPIAT) and partial pancreatectomy (PP), organoid generation, and pathologist fibrosis scoring (Fibrosis) information. For additional patient sample information see also Table S1, S2. Pancreas juice samples do not have histological sections for review and samples deemed histological failures could not be reviewed (N/A).

(C) Mutational profile of patient samples as annotated through patient medical history for which PDOs were generated. Mutations in cystic fibrosis transmembrane conductance regulator (CFTR), serine protease inhibitor kazal type 1 (SPINK1), and protease serine 1 (PRSS1) are present in our patient samples representing some of the most common alterations in CP. Mutation - a mutation was annotated in patient medical history but the specific alteration was not reported.

(D) Generation efficiency of patient derived organoids (PDOs); cumulative generation efficiency of 70.5%.

(E) Representative images of human organoid cultures established from normal (hNP) or hCP after at least 4 passages. Scale bar 500 µm.

(F) Whole mount immunofluorescence of PDOs stained with Hoechst (nuclei), EdU (pulsed for 25 hours), and CK19 (ductal marker). Scale bar 100 µm.

(G) Quantification of EdU positive nuclei in a panel of NP and CP PDOs across two or three independent experiments and multiple passages. For representative images of immunofluorescence see Figure S1D.

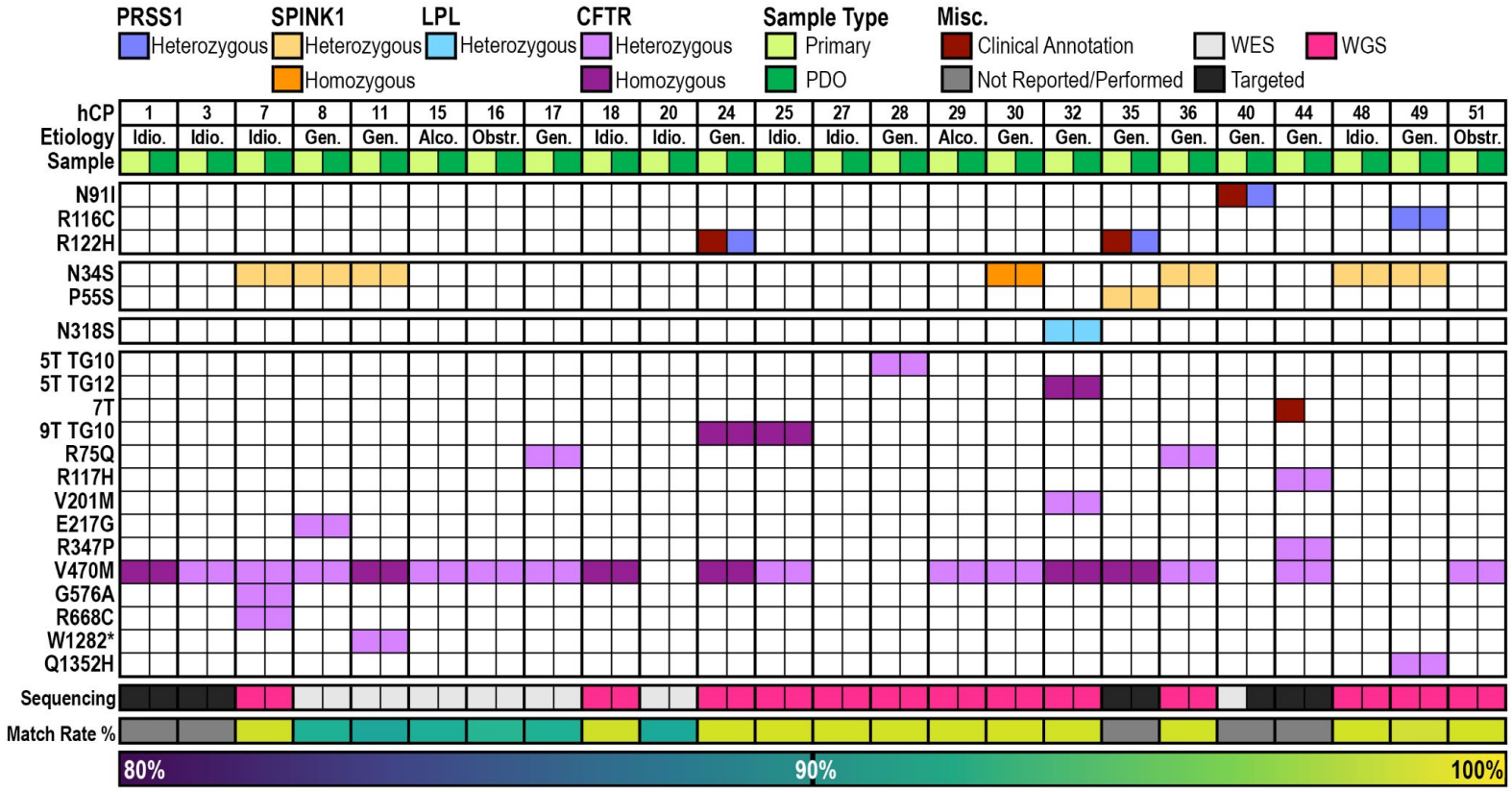

Figure 2. PDOs have high genetic concordance and reveal important and previously unannotated alterations. CP PDO and primary tissue coding sequence variants in PRSS1, SPINK1, LPL and CFTR determined from either WES (whole exome sequencing), targeted genetic sequencing, or WGS (whole genome sequencing). Genotype matches reference or is annotated as a heterozygous (Het) or homozygous (Homo) alteration as compared to reference. Clinical annotations from medical notes annotated if not found in PDO or primary tissue. Concordance is annotated for each pair of primary tissue and PDO as match rate (%). For concordance between unmatched pairs of primary tissue and PDO or PDOs see Figure S4A. For cystic fibrosis associated CFTR mutations annotated in our cohort see Figure S3B.

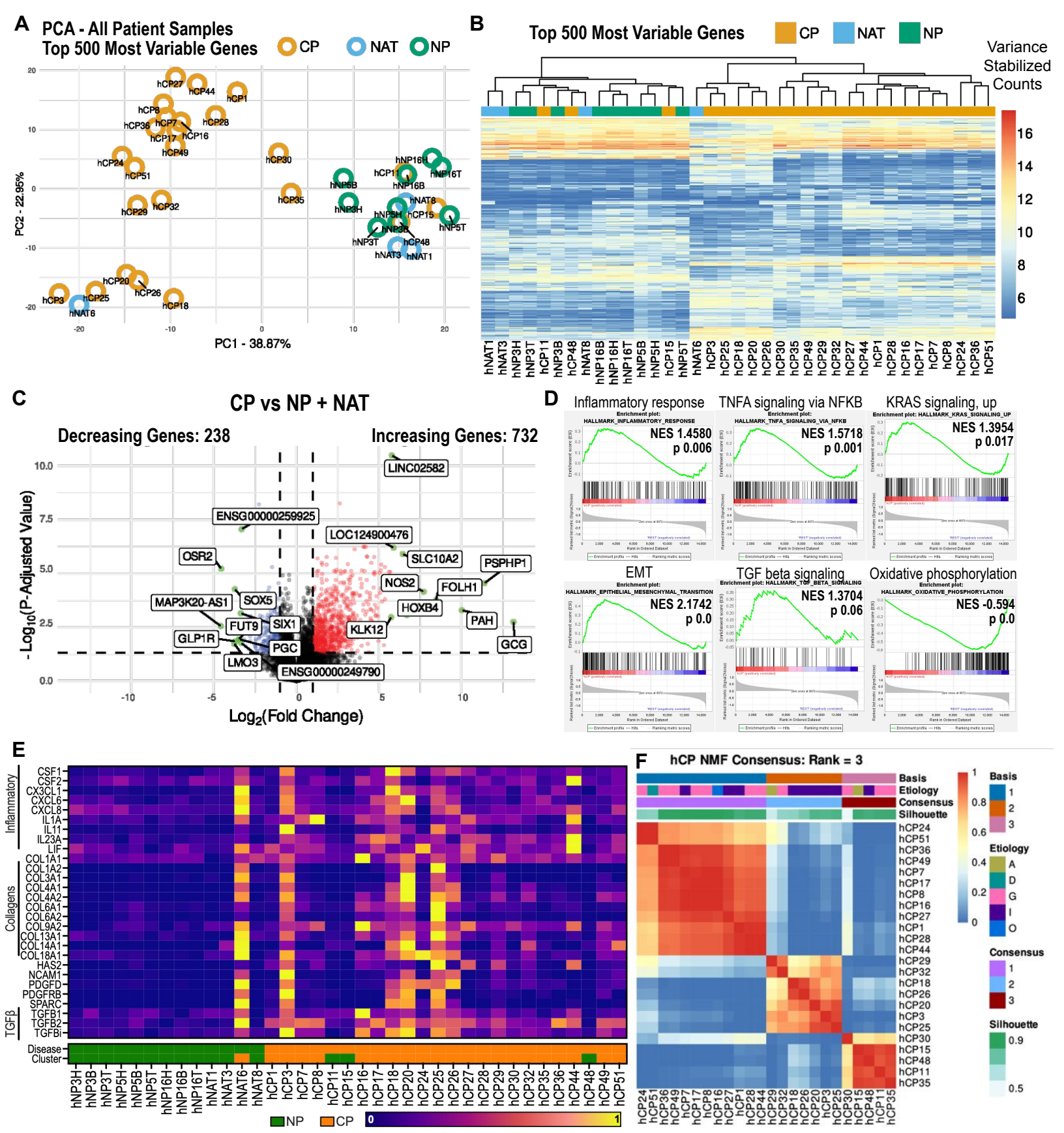

Figure 3. Gene expression analyses demonstrate distinct cell signaling programs in CP organoids.

(A) Principal component analysis (PCA) of top 500 most variable genes from organoids isolated from NP, normal adjacent to tumor (NAT), and CP samples.

(B) Top 500 variable genes from variance stabilized gene expression in hCP , hNAT, and hNP samples. Hierarchical clustering separates NP and NAT from most CP organoids.

(C) Volcano plot of CP versus NP and NAT samples. (p value <0.05, |log2fold change| > 1 colored) . Top 10 enriched or depleted genes annotated.

(D) Gene set enrichment analysis of CP PDOs versus NP and NAT PDOs.

(E) Relative normalized transcript expression of select inflammatory, collagens, and TGFb genes from RNAseq. Sample disease origin and cluster are denoted. For more information on cell lineage genes see Figure S4.

(F) Clustering using non-matrix factorization (NMF) defines three distinct subtypes of hCP PDO cultures; basis 1, 2, and 3. Patient etiology (A- alcoholic, D- divisum + groove, G- genetic, I- idiopathic, O- obstruction), silhouette, and consensus is indicated. For NMF rank survey see Figure S4.

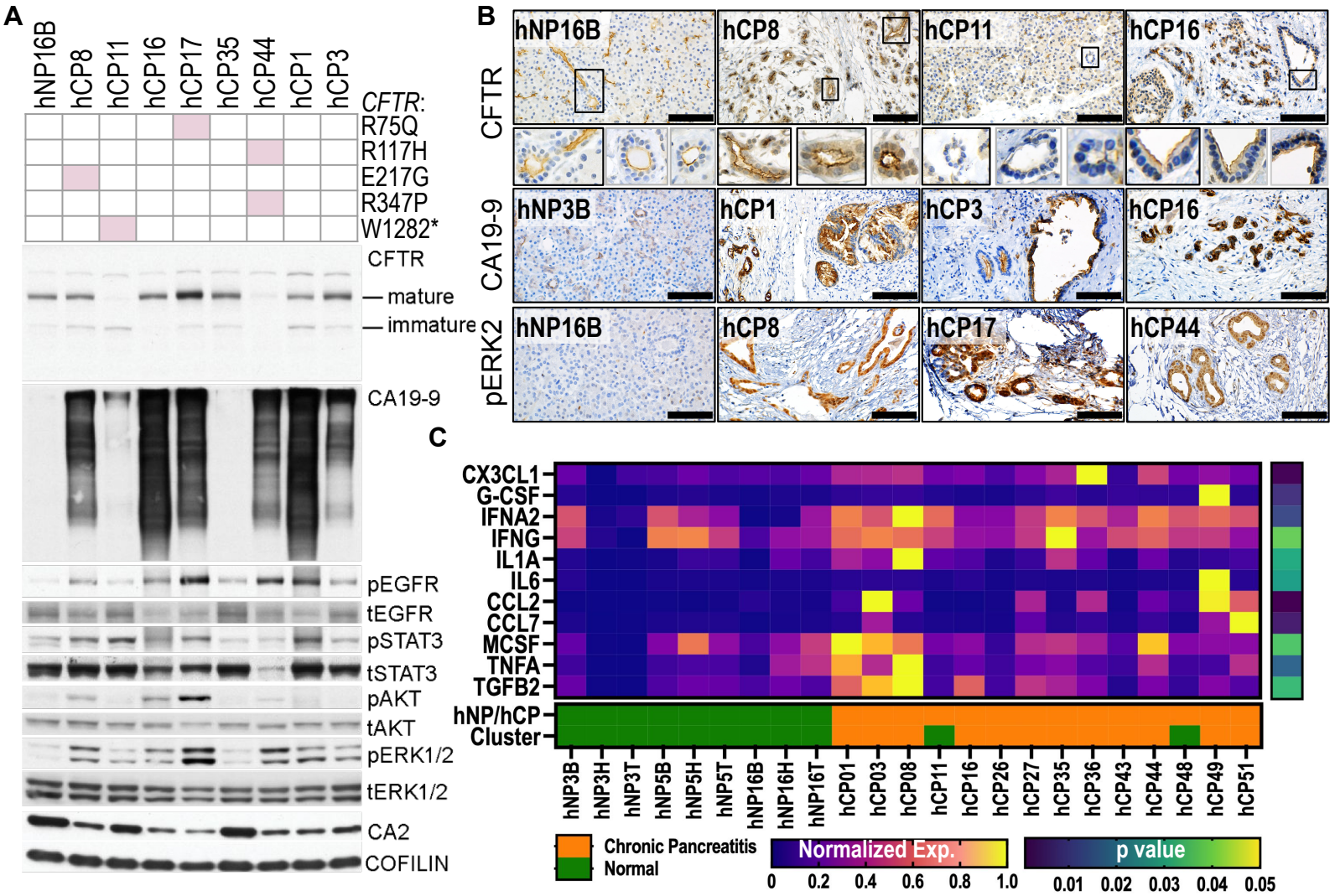

Figure 4. CP organoids recapitulate protein expression from primary tissue specimens and exhibit elevated inflammatory and mitogenic signaling.

(A) Immunoblot of PDOs generated from NP and CP samples. CFTR mutations annotated for CP samples. For normalized mature CFTR expression across cohort see Figure S7A.

(B) Immunohistochemistry (IHC) staining for cancer antigen 19-9 (CA19-9), signal transducer and activator of transcription 3 phosphorylation (pSTAT3), mitogen-activated protein kinase 1 phosphorylation (pERK2), and cystic fibrosis transmembrane conductance regulator (CFTR) of NP and CP samples. Scale bar 100 µm.

(C) Normalized secreted protein expression of inflammatory cytokines in NP and CP PDOs. Average concentration of two technical replicates per sample. P-value determined by Mann-Whitney test. Sample type and cluster is shown. For additional cytokines assayed see Figure S7B.

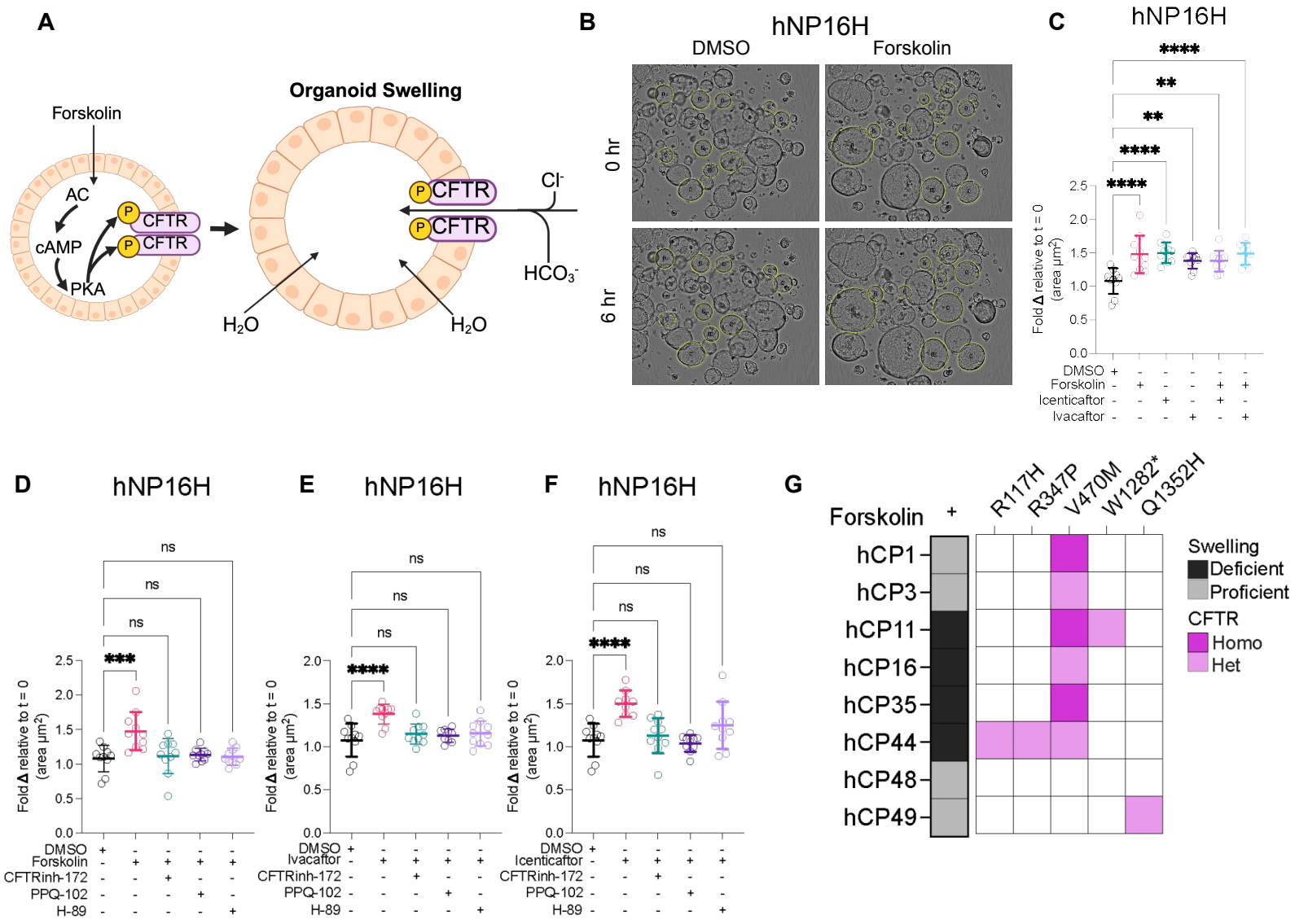

Figure 5. Forskolin induced swelling of CP PDOs is CFTR dependent.

(A) Schematic of forskolin induced swelling assay. Created in BioRender. Osorio Vasquez, V. (2025) https://BioRender.com/oahkr5p

(B) Representative brightfield images of organoids used for the quantification of forskolin induced swelling assay. Upto 10 organoids are selected per condition.

(C) Forskolin induced swelling (FIS) assay of hNP organoids with forskolin, CFTR potentiators (icenticaftor or ivacaftor), or a combination of both for 6 hours.

(D) Forskolin induced swelling (FIS) assay of hNP organoids treated with forskolin for 6 hours and pre-treated with CFTR inhibitors (CFTRi-172, PPQ-102), or protein kinase A inhibitor (H-89) for 2 hours. Swelling is inhibited with the addition of CFTR and PKA inhibitors.

(E) Forskolin induced swelling (FIS) assay of hNP organoids treated with ivacaftor for 6 hours and pre-treated with CFTR inhibitors (CFTRi-172, PPQ-102), or protein kinase A inhibitor (H-89) for 2 hours. Swelling is inhibited with the addition of CFTR and PKA inhibitors.

(F) Forskolin induced swelling (FIS) assay of hNP organoids treated with icenticaftor for 6 hours and pre-treated with CFTR inhibitors (CFTRi-172, PPQ-102), or protein kinase A inhibitor (H-89) for 2 hours. Swelling is inhibited with the addition of CFTR and PKA inhibitors.

(G) FIS assay of hCP organoids treated with forskolin for 6 hours. Data represented as swelling deficient or proficient compared to DMSO control at 6 hours. CFTR mutations are shown for each sample. Data represented as mean ± SD for C, D, E. Concentrations for forskolin treatments 20 µM, CFTR potentiators (ivacaftor, icenticaftor) or correctors (elexacaftor, lumacaftor) 10 µM for FIS assays. Data represented as swelling deficient or proficient compared to DMSO control of at least 2 independent experiments. ETI treatment concentrations are 3 µM for each compound.

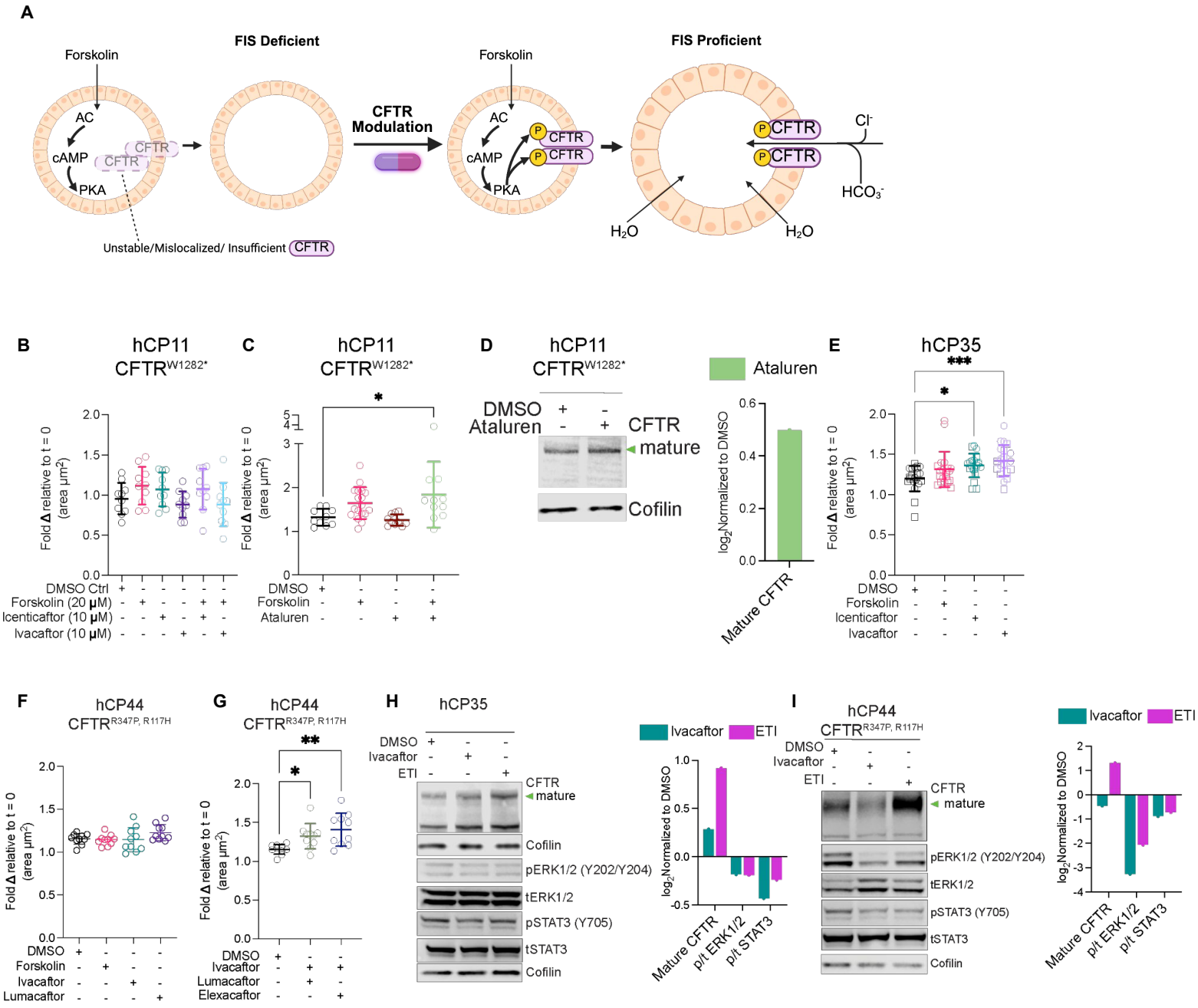

Figure 6. CFTR function in CP organoids is restored upon pharmacologic modulation.

(A) Schematic of rescuing impaired forskolin induced swelling in PDOs. Created in BioRender. Osorio Vasquez, V. (2025) https://BioRender.com/a9tuea3

(B) hCP11 (CFTR W1282*) is FIS deficient upon treatment with forskolin or CFTR potentiators (icenticaftor or ivacaftor) for 6 hours.

(C) Treatment with CFTR readthrough compound (Ataluren- 10 µM) and 6 hour treatment with forskolin in hCP11 (CFTR W1282*) induces swelling.

(D) IB of mature CFTR expression upon 48 hour Ataluren (10 µM) treatment in hCP11 (CFTR W1282*). Quantification of IB directly adjacent.

(E) FIS is rescued upon 6 hour CFTR potentiator (Ivacaftor and Incenticaftor) and forskolin treatment in hCP35 PDOs. Data representative of at least 2 independent experiments.

(F) hCP44 (CFTR R347,R117H) organoids did not swell after 6 hours of treatment with DMSO, forskolin, CFTR potentiator (Ivacaftor), or CFTR corrector (lumacaftor).

(G) hCP44 (CFTR R347,R117H) organoids swelled in response to combination CFTR potentiator (Ivacaftor) and CFTR corrector (lumacaftor or elexacaftor) treatment after 6 hours.

(H) Mature CFTR expression is increased in hCP35 organoids treated with CFTR potentiator (Ivacaftor) or further increased with ETI (CFTR correctors-Elexacaftor and Tezacaftor, CFTR potentiator-Ivacaftor) for 48 hours. pERK2 and pSTAT3 expression decreases upon ETI treatment. Cofilin is used as loading control. Representative blot of 3. Quantification of IB relative to DMSO adjacent.

(I) Mature CFTR expression increases upon ETI treatment for 48 hours (CFTR correctors-Elexacaftor and Tezacaftor, CFTR potentiator-Ivacaftor) in hCP44 (CFTR R347,R117H) organoids. pERK1/2 and pSTAT3 is signaling is decreased upon ETI treatment. Cofilin is used as loading control. Quantification of IB relative to DMSO adjacent. Data represented as mean ± SD for C, D, E. Concentrations for forskolin treatments 20 µM, CFTR potentiators (ivacaftor, icenticaftor) or correctors (elexacaftor, lumacaftor) 10 µM for FIS assays. Data represented as swelling deficient or proficient compared to DMSO control of at least 2 independent experiments. ETI treatment concentrations are 3 µM for each compound.